CNT FIELD EMISSION CELL WITH BUILT-IN ELECTRON BEAM SOURCE FOR ELECTRON STIMULATED AMPLIFIED FIELD EMISSION

By

Nikkon Ghosh

Thesis

Submitted to the Faculty of the

Graduate School of Vanderbilt University

in partial fulfillment of the requirements

for the degree of

MASTER OF SCIENCE

in

Electrical Engineering

August, 2008

Nashville, Tennessee

Approved:

Professor W. P. Kang

Professor J. L. Davidson

To my family

ACKNOWLEDGEMENTS

First of all, I would like to thank my academic and research advisor, Prof. W.P. Kang for his assistance, guidance and encouragement throughout my study at Vanderbilt University. I would like to express my appreciation to Prof. J. L. Davidson for his assistance and recommendations on my research. I would also like to thank Mr. Mick Howell, Dr. Yong Mui Wong (Kelvin) and Dr. B. K. Choi for their diverse discussions and assistance in my work. I am also thankful to my colleagues to keep the work going.

Finally I would like to express my sincere appreciation for my parents, my sister, my uncle-aunty and Anindita, whose constant support made me persistently strong during difficult moments.

TABLE OF CONTENTS

Page

Appendix

ABSTRACT

Carbon Nanotube (CNT) is an emerging form of carbon nanostructure, vastly expanding its utility for several applications ranging from electronics to tribology. CNT is an excellent material for electron field emission due to its high aspect ratio, robust mechanical and chemical properties, high thermal conductivity, and ability to withstand high temperature and ion bombardment. This research is focused on the fabrication and characterization of a novel CNT field emission cell with a built-in electron beam source for electron excited amplified field emission. In brief, reliable and consistent process techniques have been developed to grow aligned CNTs under different growing conditions using MPCVD. This process was integrated in the fabrication of monolithic lateral field emission cell (FEC) in diode configuration with a built-in electron beam source. Field emission behaviors with and without activation of the built-in electron beam were characterized. A high voltage of 1.8 kV was applied to generate the bombarding electron beam on the FEC. The emission current of the FEC increases markedly with the activation of the electron beam source due to impact ionization and direct interaction with the FEC CNT cathode. The emission behaviors were confirmed by F-N plots. It was found that ~ 10 times current amplification was achieved. These results demonstrate the feasibility of a novel means of power generation using electron stimulated impact ionization field emission.

LIST OF TABLES

LIST OF FIGURES

CHAPTER I

INTRODUCTION

Carbon Nanotubes

Carbon nanotubes (CNTs) are allotropes of carbon with a nanostructure that can have a length-to-diameter ratio greater than 1,000,000 [1]. These cylindrical carbon molecules have novel properties that make them potentially useful in many applications in nanotechnology, electronics, optics and other fields of materials science, as well as extensive use in arcology and other architectural fields. They exhibit extraordinary strength and unique electrical properties, and are efficient conductors of heat. The nature of the bonding of a nanotube is described by applied quantum chemistry, specifically, orbital hybridization. The chemical bonding of nanotubes is composed entirely of sp^2 bonds, similar to those of graphite. This bonding structure, which is stronger than the sp^3 bonds found in diamond, provides the molecules with their unique strength. [1]

The discovery of nanotubes remains a contentious issue. Many believe that Iijima's report in 1991 is of particular importance because it brought carbon nanotubes into the awareness of the scientific community as a whole. Carbon nanotubes have been produced and observed under a variety of conditions prior to 1991. A paper by Oberlin, Endo, and Koyama published in 1976 clearly showed hollow carbon fibers with nanometer-scale diameters using a vapor-growth technique [2]. Additionally, the authors show a TEM image of a nanotube consisting of a single wall of graphene. Later, Endo has referred to this image as single-walled nanotubes [3]. Carbon-based nanostructured

materials still continue to attract a disproportionate share of research effort because of their wide-ranging applications. Potential applications of CNTs include microcathodes for vacuum field emission displays [4], electron source for vacuum electronics [5], microwave power amplifier [6], gas sensors for chemical sensing[6], scanning probe for atomic force microscope [7], wires for quantum electronics [8], hydrogen storage for fuel cells [9], electrodes for discharge tubes[10], electrochemical capacitor for high power[11], nonvolatile random access memory for molecular computing[12], nanotweezers for microelectrochemical systems (MEMS) [13] and semiconductor for solid state nanoelectronics [14].

There has been a tremendous amount of work studying defect-free nanotubes, including single or multiwalled nanotubes (SWNTs or MWNTs). A SWNT is a hollow cylinder of graphite sheet with hexagonal structural feature whereas a MWNT is a group of coaxial SWNTs. A SWNT can be visualized as a hollow cylinder, formed by rolling over a graphite sheet, as shown in Figure 1.1. Three typical nanotubes can be obtained: zigzag (n, 0), armchair (n, n) and chiral (n, m) where n>m>0 by definition [1]. The detailed structure of nanotubes is mentioned elsewhere [15]. In addition to defect-free nanotubes, observed structures also include the capped and bend, branched, and helical MWNTs [1], and the bent, capped and toroidal SWNTs [1]. Most of these structures are believed to have topological defects such as pentagon or heptagon incorporated into the nanotubes of hexagonal network. Till date, different methods to synthesize CNTs have been reported by different groups, which has mentioned in appendix B.

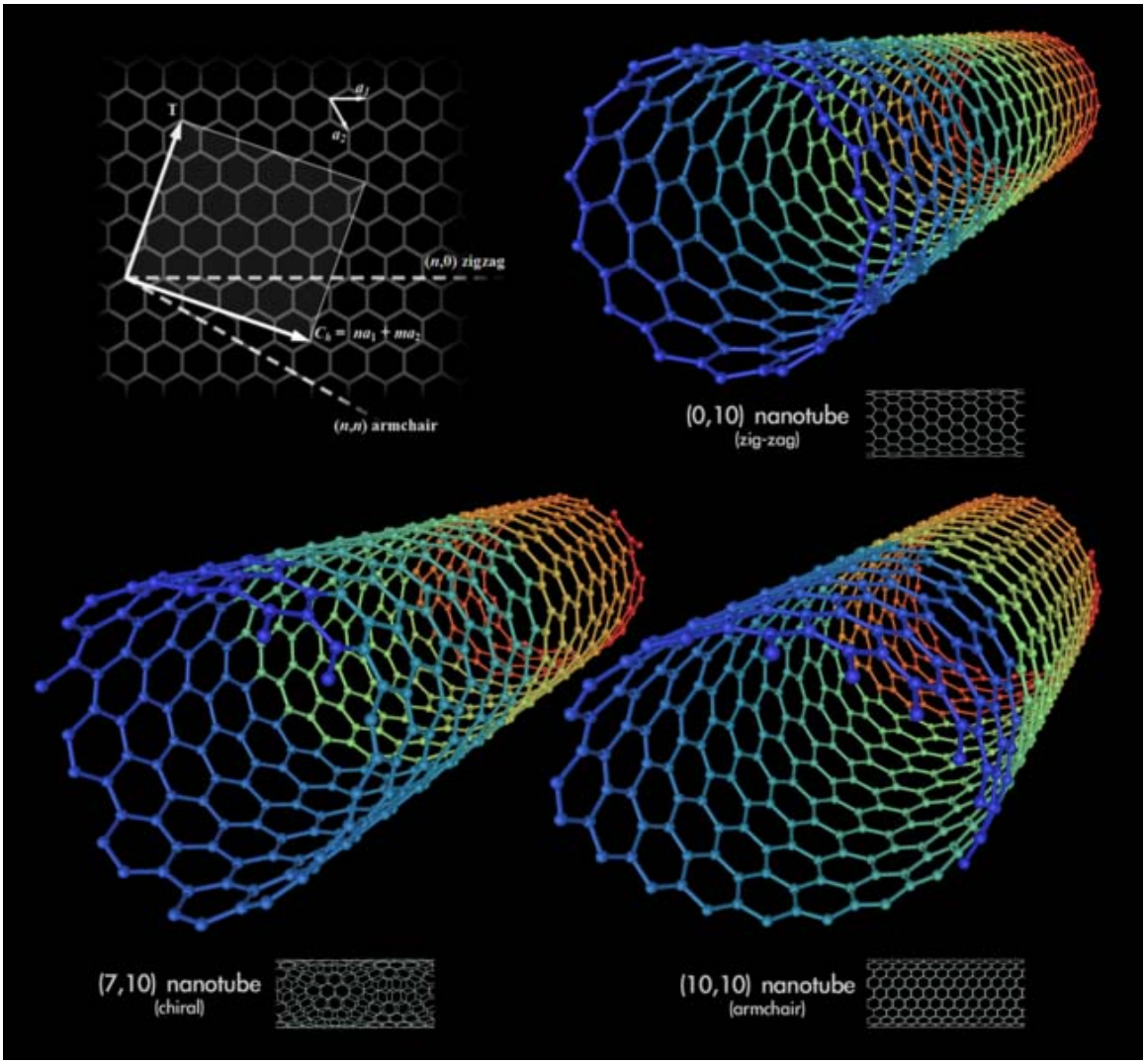

Figure 1.1: 3D model of three types of single-walled carbon nanotubes. By rolling a graphite sheet in different directions, these typical configurations can be obtained: zigzag (n, 0), armchair (n, n) and chiral (n, m) where n>m>0 by definition. In this specific example, they are (10, 0), (10, 10) and (7, 10) respectively.

Vacuum Field Emission

We have mentioned that CNT has potential applications in vacuum field emission. So what is vacuum field emission? Field emission (FE) is the emission of electrons from the surface of a condensed phase into another phase due to the presence of high electric fields. If this phenomenon takes place under vacuum then it is called Vacuum Field Emission (VFE). In this case, electrons quantum-mechanically tunnel through the surface potential barrier (work function) into vacuum [16]. VFE devices are sometimes referred to Vacuum Microelectronics (VME) devices. These devices capitalize on the electron transport through vacuum [16]. Figure 1.2 shows the basic structural difference between the solid state MOS transistor and vacuum triode transistor. Some of the advantages of VFE devices over solid-state are:

- Electrons travel through vacuum with less energy dissipation than solid-state semiconductor devices.
- Insensitive to temperature and radiation. Whereas in solid-state microelectronic devices, signal and device performance degradation are one of the major concerns because of electron scattering transport in the semiconductors.
- Switching speed is extremely fast, limited by speed of light ~ 3×10^8 m/s. In case of solid-state microelectronic devices it is limited by the carrier saturation velocity, ~ 1×10^5 m/s in Si and GaAs, and ~2×10^5 in GaN.
- High output power.

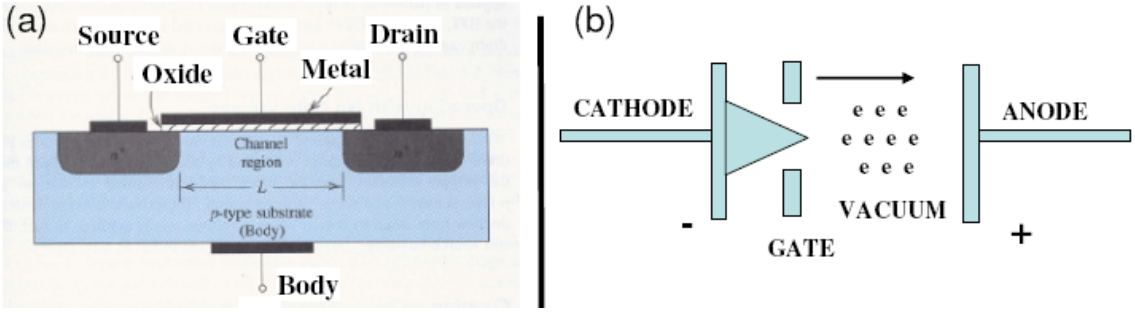

Figure 1.2: Schematic cross section of (a) solid-state MOS transistor and (b) vacuum triode transistor.

To date, fabricated and proposed field emission devices (FEDs) have been largely divided into two categories: vertical and lateral. Lateral field emitters are easier to fabricate over vertical field emitters with attractive design versatility of electrode geometry and has attractive applications for low turn-on field devices [17]. In addition, due to small inter-electrode overlapping area, the device input capacitance of lateral FEDs is inherently small [17]. As a result, lateral devices are able to draw significant amount of research attention. Figure 1.3 shows both the lateral and vertical devices grown by Vanderbilt University using CVD diamond and CNTs as emitter.

Spindt and coworkers, in 1968 developed micro field emitter array (FEA) by thin film deposition of molybdenum (Mo) cones on Si substrate. Later, to take the advantages of the advances in photolithography and micro fabrication technology, the work on FEA was extended to silicon microtips. But higher cost of fabrication and high cathode sensitivity to the contaminations made both types of FEAs less applicable. As a result, researchers have been looking for other field emission cathode materials, mainly allotropes of carbon such as diamond, carbon nanotubes and etc.

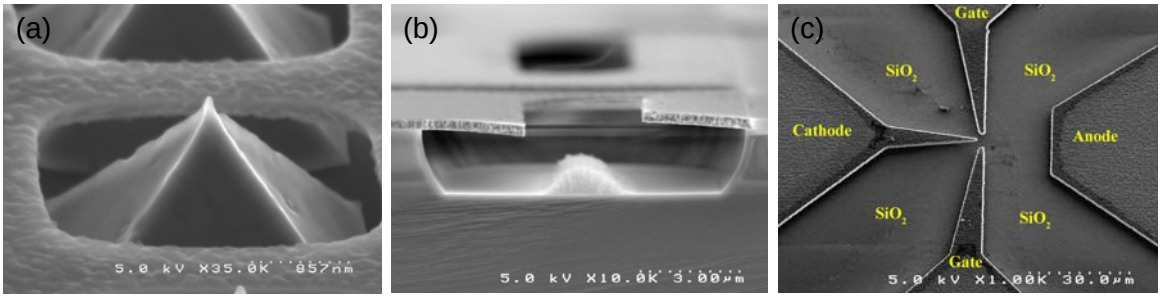

Figure 1.3: SEM micrograph of typical (a) vertical field emission devices with CVD diamond as emitter, (b) vertical field emission devices with CNTs as emitter and (c) Lateral field emission devices with CVD diamond as emitter by Vanderbilt.

Due to its low or negative electron affinity (NEA), diamond is one of the promising candidates as a cold cathode emitter. The conduction band edge of hydrogen-terminated diamond lies above the vacuum level. As a result, low threshold field of 3-40 V/μm for a current density of 10 mA/cm^2 can be achieved with diamond as emitter [18]. Great interests have been shown in CVD diamond for VME applications partly due to the ability of depositing diamonds by low pressure chemical vapor deposition (CVD) technique. Typical diamond microtips fabricated by Vanderbilt University are shown in Figure 1.3 (a) and (c).

On other side, CNTs have displayed extraordinary electro-mechanical properties, thermal and chemical stability. Most importantly, due to high aspect ratio, CNTs has been shown to be excellent field emitters with low turn on and threshold field. Although The work function of CNT is relatively high (5.5 eV), the sharp nanotips help electrons to overcome the surface potential barrier at low microscopic field due to high field enhancement at the tips. Figure 1.3 (b) shows the CNT vertical field emission devices. In addition, CNTs are the center of researchers' attention for numerous VME applications

because of its ability to deliver high current density in excess of 1 A/cm^2 [19]. An overview of carbon nanotubes' property can be found in Appendix A.

Objective of the research

The scope of this study is limited to electron field emission of multi-walled carbon nanotubes (MWNTs) grown by microwave plasma enhanced chemical vapor deposition (MPCVD). The research was mainly focused on:

- Selective growth of CNTs using cobalt (Co) catalysts on patterned substrate.
- Studying the change in CNTs structure by changing growth parameters.
- Synthesis of CNTs by MPCVD.
- Implementation of electron beam lithography (EBL) to get micro patterned device structure.
- Characterization of the fabricated CNT field emitter cell in diode configuration.
- Characterization of the fabricated CNT field emitter cell under the influence of electron beam as external stimulator.

Organization of the thesis

The thesis consists of five chapters and appendices:

- Chapter 1 gives an introduction on carbon nanotubes and vacuum field emitter devices. In addition, the objective of this research is mentioned.
- Chapter II gives a detail elaboration on synthesis of CNTs under different growing conditions.
- Chapter III contains the study of field emission and electron beam amplified field emission.
- Chapter IV provides summary and conclusion of the studies described in 2nd and 3rd chapters.
- Chapter V provides recommendations for future works of this research.
- Appendices

    A. Structure and Properties of Carbon Nanotubes.

    B. Growth mechanism and Synthesis of CNTs.

    C. Electron beam lithography.

CHAPTER II

SYNTHESIS OF CNTs

Introduction

This chapter explores the effect of various growth parameters on CNT synthesis. In past, several groups have studied the control of CNT orientation and synthesize by CVD for various catalysts [20-21], gas sources [22-23] and substrates [24]. The roles of different catalyst particles, reaction temperature and reaction gases in CNT synthesis have been studied [25-26]. In our previous studies, MPCVD was successfully used to synthesize multi-walled vertically aligned CNTs by using CH_4-H_2 gas mixture [27]. It was found that microwave power and working temperature affect the growth rate [27]. In this part of the research, the influence of important parameters including gas flow rate, buffer layer thickness, growth temperature, applied microwave power, pretreatment time, growth time and substrate biasing, on the alignment and morphologies of the synthesized CNTs were studied systematically.

Experiment

Five sets of experiments were performed to examine the role of different physical parameters on the growth of CNTs. The physical parameters were varied and their values listed in Table 1. For all set of experiments, an ASTEX 1.5 kW MPCVD system equipped with induction heater for substrate heating was used to grow CNTs. Highly doped N^+ type silicon substrates (100) of resistivity 0.002-0.0035 Ω-cm were first coated

with a thin layer of titanium (Ti) followed by the catalyst, cobalt (Co), with a shadow mask using DC magnetron sputtering under a vacuum of ~$5x10^{-5}$ Torr [22]. The Ti acts as a diffusion barrier layer for the catalysts to prevent the formation of silicide at high temperature [28].

The first experiment, samples A1-A6, can be divided into three groups having two samples each with the same thickness of buffer-catalyst (Ti-Co) layer. The samples from each group were subjected to different working temperature, while the remaining parameters were kept unaltered. In exp. 2, sample B1-B4, the thickness of buffer catalyst layer was kept constant and N_2 was introduced. There is another important difference between exp. 1 and 2. In the first experiment the substrates were pretreated only by H_2 plasma, whereas, in the second experiment there was no plasma treatment but heat treatment in H_2 environment for longer period of time. The intension was to study the effect of these two changes on CNT synthesis. In experiments 3-5, the samples were subjected to plasma as well as heat treatment in sequence. In addition, a negative bias of 100 volt was also applied to the substrates. Each of the experiments consists of 4 samples with catalyst (Co) thickness 4 nm, 10 nm, 15 nm and 20 nm respectively while the buffer layer (Ti) thickness was kept constant at 20 nm. In the third and fourth experimental set, no physical parameters were changed except the order of the experiments. In experiment 3, H_2-N_2 plasma was turned on after the pretreatment time followed by the bias and methane (CH_4) introduction initiate CNT synthesis for 10 min. But in the next two set of experiments this order has been modified. The bias was applied right after the pretreatment and then the H_2-N_2-CH_4 plasma was turned on to initiate the CNT growth. Last, in the fifth experiment higher microwave power of 1 kW was applied.

Experimental Results and Discussions

The CNT morphologies such as vertical alignment, average tube diameter, height and amorphous carbon (a-C) nanoparticles content of all the samples were observed and analyzed with a Hitachi 4200 scanning electron microscope (SEM).The growth mechanism of CNTs is believed to occur via decomposition of the carbonaceous gas molecules at the surface of catalyst nanoparticles, and diffusion of carbon atoms through the nanoparticles [28]. Throughout the experiments hydrogen was used to dilute the hydrocarbon (CH_4) to reduce the amorphous carbon deposition on the tips of CNTs. In experiment 1, the effects of the growth temperature, and different catalyst and buffer layer thicknesses were investigated. Samples A1-A6 were all pretreated with H_2 plasma for 5 min at the respective growth temperature. It has been shown that plasma pretreatment prior to CNT growth is important in synthesizing aligned CNTs due to the formation of uniform catalytic nanoislands [21, 17]. In addition, the H_2 plasma pretreatment also tend to reduce accumulation of a-C nanoparticles on the CNT walls during the initial synthesis stage, resulting in CNTs with better quality [4, 17].

As observed in Figure 2.1, the as-grown CNTs are generally well aligned and contain few carbon nanoparticles. The catalyst layer thickness just varied by 2 nm. Since tube diameter is dependent on thickness of catalyst layer, there is a small change in average diameter, from 10 nm to 30 nm. Among the three groups, the thicknesses of the buffer-catalyst layer were varied while keeping all the other parameters constant. Consequently, appropriate buffer layer thickness for the 2 nm thick catalyst layer is found to be 10 nm. Among the three groups in the first experiment, sample A3 and A4 have better physical alignment. The working temperature was found to play a crucial role.

Specifically, it affects CNT' height and alignment. It has been observed that the CNTs grown at higher temperature, i.e. 700 ^{0}C are shorter than those grown at 650 ^{0}C. On the average, samples synthesized at 650 ^{0}C have 2 – 5 μm taller nanotubes than those of at 700 ^{0}C. Here, two different temperatures were applied with the intension to find out the more appropriate value to grow well aligned nanotubes. Overall in experiment 1, sample A3 has the best alignment with height and diameter 10 μm and 20 nm respectively.

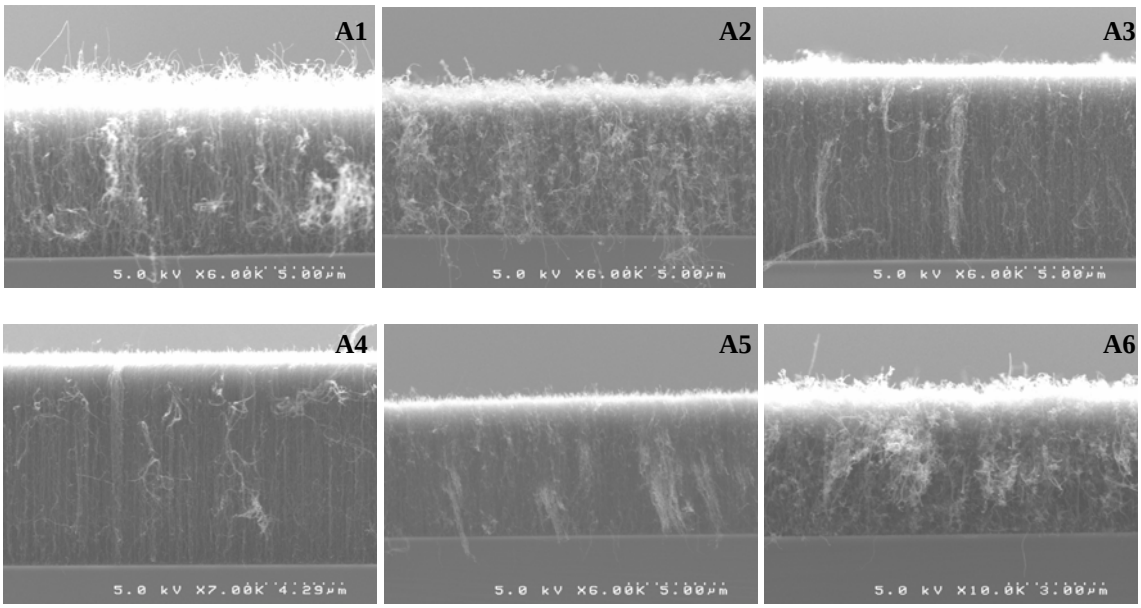

Figure 2.1: SEM images of CNTs with different catalyst thickness and temperature (Exp. No. 01).

In experiments 2 - 5, heat treatment was introduced and longer time was required to breakdown the catalytic thin film into nanoparticles. Due to longer pretreatment time thicker buffer layer was used to prevent silicide formation. In addition, N_2 was introduced at lower pressure to investigate the combine influence on the growth mechanism of CNTs. In the second experiment, the samples were only heat-treated in H_2 ambient

without plasma pretreatment for 15 min. It was found that at higher concentration of N_2, ball-like carbon particles were obtained (Figure 2.2-B3).

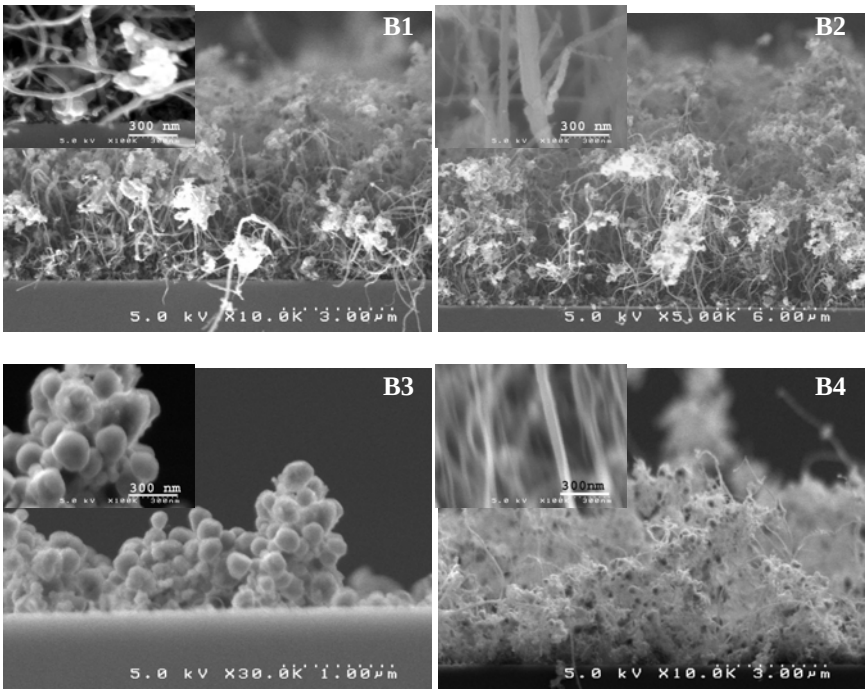

Figure 2.2: SEM images of CNTs with different N_2 flow rates (Exp. No. 02). Sample B1, B2 and B3 were exposed to 5, 10 and 15 sccm of N_2 respectively. Sample B2 and B4 were subjected to same parameters/growth condition, except the later one had longer heat pretreatment time. Inset shows the high magnification image of the same sample.

However, at low N_2 concentration CNTs were obtained but granular ball-like and amorphous carbon also appeared in the mix, Figure 2.2-B1, B2 and B4. Furthermore, sample B4 has more granular and sheet-like amorphous carbon structure at the top compared to sample B2 due longer heat treatment time. This phenomenon can be explained from the growth model for a tip-type CNTs. According to this model carbon precipitation takes place on the opposite surface of the catalyst particle to form the

nanostructure while the particle remains on the top throughout the growth and bigger the particle size, poorer the nanostructure's alignment [28]. Presence of such catalyst particles can easily be noticed on the tips of the samples.

It seems that only heat pretreatment is not enough to grow aligned CNTs, so from the next experiment onwards both types of pretreatments were introduced. It has also been observed that at lower pressure (13 Torr), the plasma at 1 kW microwave power was relatively unstable compared to the higher pressure (20 Torr) used in experiment 1. In experiments 3-5, a negative bias of 100 V was applied to the samples during the MPCVD growth. It has been shown that the effect of a negative bias on the substrate is beneficial for achieving highly aligned and dense CNTs [29]. It is clear from the SEM images that sample C1; Figure 2.3 the one with the thinnest catalyst layer has much better aligned CNTs with almost no nano-carbon or ball-like particles on the top surface. However the carbon contamination increases from sample C1 to C4. The thicker Co layer which resulted in bigger and heavier nanoparticles after the pretreatment [4, 21] might have led to poorer vertical alignment of the CNTs. It has also been observed that carbon contamination on top of CNTs can be reduced by turning off the carbon containing gas few seconds before switching off the plasma, because H_2 plasma etches away the deposited nanocarbon particles once the gas flow of carbon feedstock is stopped [28]. It is believed that due to the applied bias [30] and very short plasma pretreatment time [31, 32], for samples C1-C4 with different catalyst layer, the CNTs are found to have almost the same height, 20μm, almost uniform diameters, ranging from 35 – 45 nm and moderate aligned.

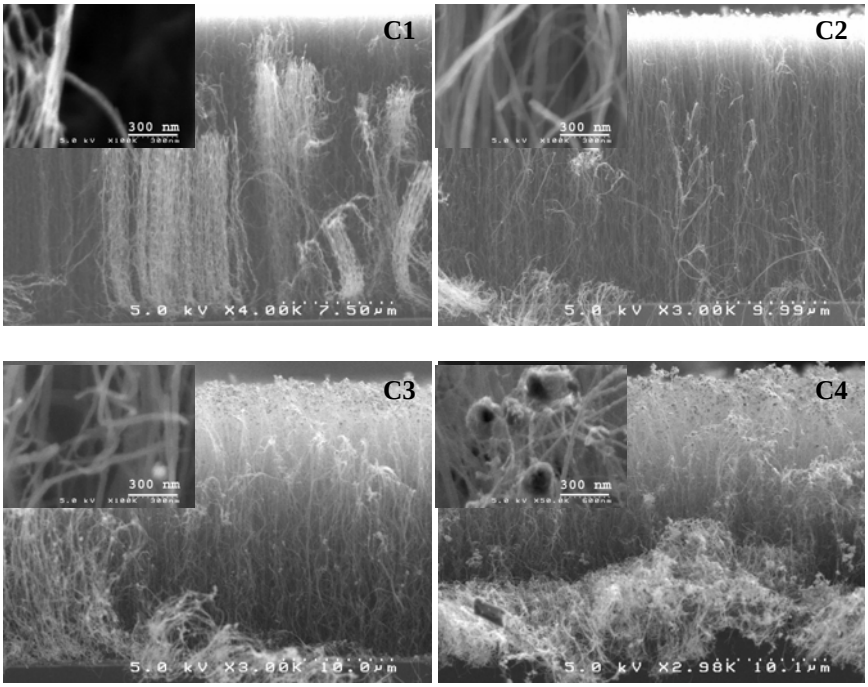

Figure 2.3: SEM pictures show the effect of catalyst film thickness (Exp. 03) on the structure on the CNTs. The buffer layer thickness was kept same (refer table 1 for more details). Inset shows the high magnification image of the same sample.

In experiments 4 and 5, the experimental order was modified with the expectations to achieve taller and well aligned nanotubes. Specifically, the negative bias was applied right after the H_2 heat pretreatment followed by H_2-N_2-CH_4 plasma to initiate the CNTs growth. Whereas in the previous experiments, H_2-N_2 plasma was started after the pretreatment, followed by the bias and lastly CH_4 was introduced to initiate the growth. The variation in the experimental order was designed to observe changes, if any, in the CNT structure and alignment.

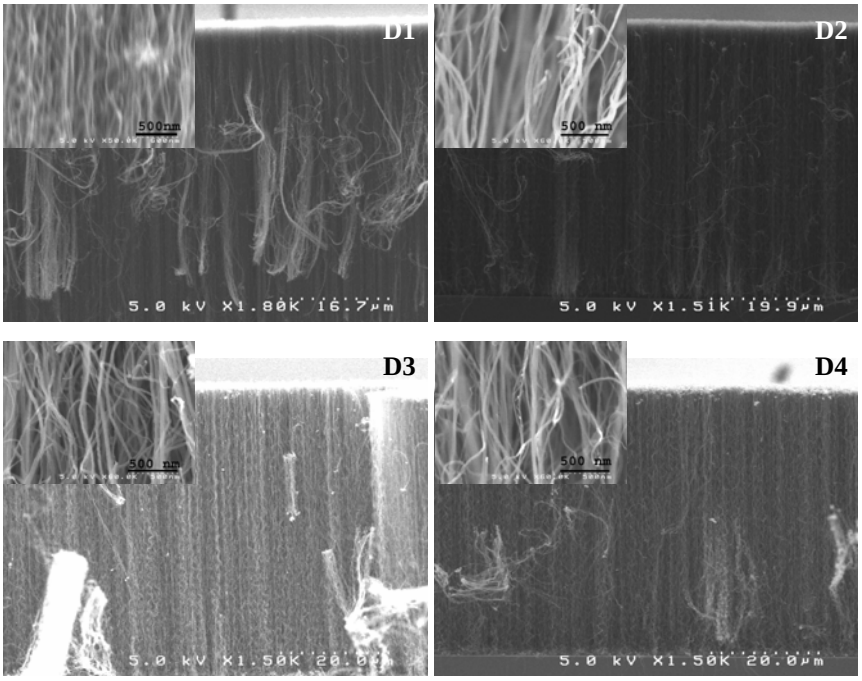

Figure 2.4: SEM micrograph of the synthesized CNTs at lower power, 400 watt (Exp. 04). The order of the experiment can be given as; PT→ HT→BIAS→$H_2/N_2/CH_4$ PLASMA. Inset shows the high magnification image of the same sample.

In the fourth experiment, the CNTs are found to be much more aligned and almost no nano-carbon particles on the top (Figure 2.4-D1, D2, D3 and D4). Furthermore, the CNTs are found to have almost the same height, 50µm but non-uniform diameters, ranging from 30 – 50 nm for samples D1-D4 with different catalyst thickness. Whereas in the third experiment, the CNTs are not well aligned, shorter in length by at least 20µm and contain lots of nano-carbon particles. These significant changes are observed most probably due to the change in the experimental order [30] as mentioned before.

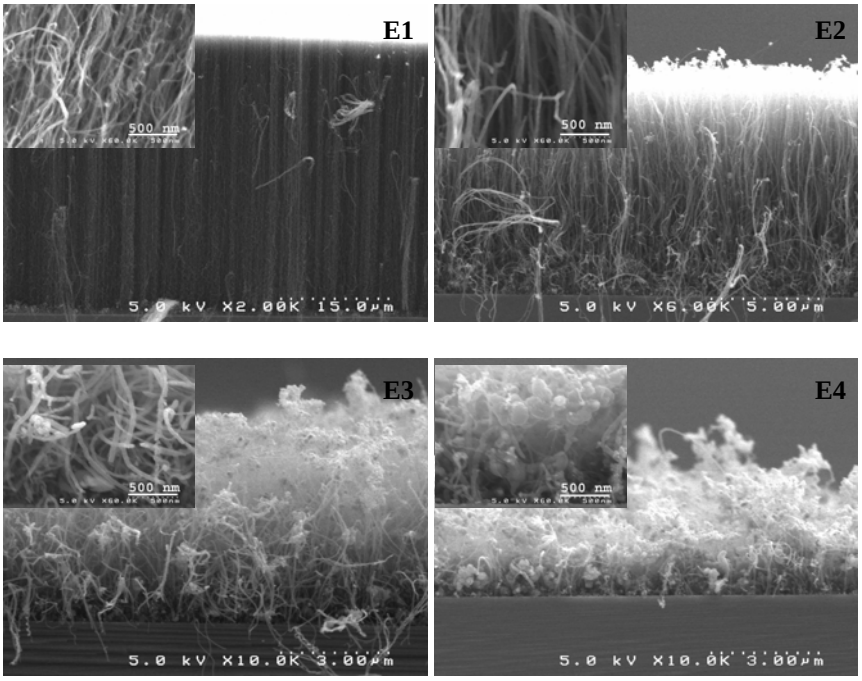

Figure 2.5: SEM micrograph of the synthesized CNTs at higher power, 1000 watt (Exp. 05). The order of the experiment was same as the previous one. Inset shows the high magnification image of the same sample.

In the fifth experiment higher microwave power of 1kW was applied. It is observed that CNT quality differs with the catalyst size (Figure 5-E1, E2, E3 and E4), i.e. thinner catalyst layer improves the CNT alignment. Also the average diameter and height change dramatically with different catalyst thickness. Sample E1 has almost the same diameter and height as previous experiment, sample D1-D4. It is proposed that the growth of CNTs for lighter particle size may be invariant of the applied microwave power. Since the nanoparticles remain at the top throughout the growth, bigger and heavier nanoparticles may require more precise parameters such as higher microwave power and heavier plasma gas to synthesize aligned CNTs [28]. For the rest, E2-E4 the height ranges from 5 – 15 μm and diameter from 50 – 80 nm. This difference in height

and diameter is most likely due to the higher momentum of the particles in the stronger plasma which give rise to a greater bombardment energy and temperature to melt more catalytic nanoparticles to form bigger islands [33].

Table 1: Specific details of the synthesis parameters used to grow CNTs. The parameters include buffer/catalyst thickness, temperature (T), pressure (P), power (E), flow rates, plasma treatment (PT), heat treatment (HT), growth time and bias.

Exp No.	3 mm dot Sample	Catalyst Ti/Co				Flow rate			Pretreatment Time		Growth Time	Bias
			T	P	E	H_2	CH_4	N_2	PT	HT		
		nm	^{0}C	Torr	Watt	SCCM	SCCM	SCCM				V
1	A1	10/4	650	20	400/1000	120	15	-	5m	-	3m	-
	A2	10/4	700	20	400/1000	120	15	-	5m	-	3m	-
	A3	10/2	650	20	400/1000	120	15	-	5m	-	3m	-
	A4	10/2	700	20	400/1000	120	15	-	5m	-	3m	-
	A5	4/2	650	20	400/1000	120	15	-	5m	-	3m	-
	A6	4/2	700	20	400/1000	120	15	-	5m	-	3m	-
2	B1	20/20	700	13	1000	135	15	5	-	15m	10m	-
	B2	20/20	700	13	1000	135	15	10	-	15m	10m	-
	B3	20/20	700	13	1000	135	15	15	-	15m	10m	-
	B4	20/20	700	13	1000	135	15	10	-	30m	10m	-
3	C1	20/4	700	20	400	135	10	15	5s	30m	10m	-100
	C2	20/10	700	20	400	135	10	15	5s	30m	10m	-100
	C3	20/15	700	20	400	135	10	15	5s	30m	10m	-100
	C4	20/20	700	20	400	135	10	15	5s	30m	10m	-100
4	D1	20/4	700	20	400	135	10	15	5s	30m	10m	-100
	D2	20/10	700	20	400	135	10	15	5s	30m	10m	-100
	D3	20/15	700	20	400	135	10	15	5s	30m	10m	-100
	D4	20/20	700	20	400	135	10	15	5s	30m	10m	-100
5	E1	20/4	700	20	1000	135	10	15	5s	30m	10m	-100
	E2	20/10	700	20	1000	135	10	15	5s	30m	10m	-100
	E3	20/15	700	20	1000	135	10	15	5s	30m	10m	-100
	E4	20/20	700	20	1000	135	10	15	5s	30m	10m	-100

CHAPTER III

FABRICATION OF LATERAL CNT FIELD EMISSION ENERGY CONVERSION CELL

Introduction

In previous section we have reported growing vertically aligned CNTs by controlling the thickness of the catalyst, using microwave plasma enhanced chemical vapor deposition (MPCVD). This chapter describes how CNT emitters were synthesized selectively on a single chip as electron emitters for both a field emission cell and an external electron beam source. The goal of this work is to study how electron emission of a field emission cell (FEC) can be stimulated by an external electron beam hitting the emitting CNTs. The probability of the electron tunneling can be greatly increased by several methods, e.g. local field enhancement through sharp emitting tips [35], work function lowering material coating [36] or supply of external energy to lower the surface potential barrier [37, 38, and 39].

In this work, an energized electron beam was used to supply the external energy to the emitting CNTs by bombarding electrons [17] to achieve amplified emission current. This concept is very much similar to photofield emission in terms of electron-hole pair generation. Briefly, in the photoemission process, if an electron absorbs the energy of one photon and has more energy than the work function, it is ejected from the material [28]. If the photoemission process is combined with an applied field, the effective work function of the cathode can be reduced, resulting in much higher emission current [38]. It is well-known that field emission, a quantum mechanical tunneling process, is a surface phenomenon which depends on the potential barrier of the solid-

vacuum interface involving extraction of electrons by intense electric field [16]. It is also known that if an electron with energy greater than the bandgap energy (E_G) hits a semiconductor, it breaks semiconductor-semiconductor bond and generates electron-hole pairs [39, 40] and if they are pulled out of the material by an applied electric field then amplified emission current is achieved. But if there is no field to extract the generated electron then it recombines again and during this process it emits a photon [41, 42], Figure 3.1. If the electron is exited to higher energy level in conduction band then it first comes to the lowest energy level in conduction band by emitting a phonon and finally jumps back to valance band to recombine. Whereas in metal, there is no electron-hole pair generation by the external excitation, instead the electrons from the Fermi level moves up to higher energy state and then comes back to the lower energy state by emitting a phonon under the absence of electric field. The surface potential barrier of CNTs [35] being higher than other emitters, ~5 eV, the electrons couldn't overcome the potential height easily without electric field. So, the conduction band electrons generated by external energy, tunnel into vacuum only under an appropriate applied field, as illustrated in Figure 3.2 (d) and (e). The bandgap energy of semiconducting CNTs being relatively small, less than one electron volt, it's comparatively easy to generate more charge carriers in conduction band than any other emitters [1, 28]. As a result, under the same applied field more electron tunnel from CNTs to vacuum and hence higher current in the FEC is noticed.

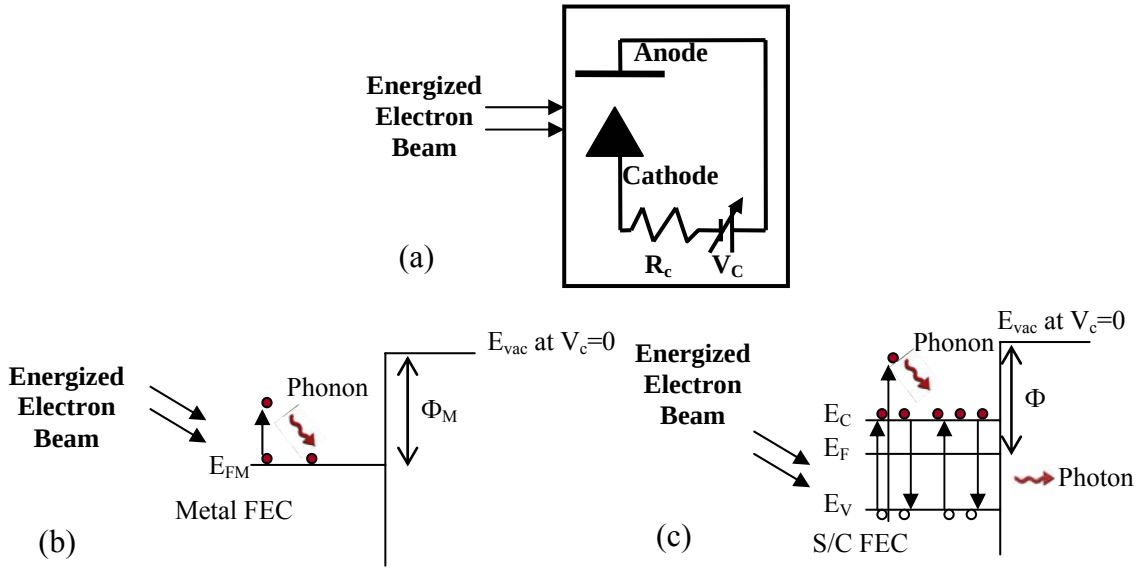

Figure 3.1: (a) Field emission cell with V_c = 0 but under energized electron beam. Corresponding energy band diagram of (b) metal and (c) semiconductor FEC cathode bombarded by external e-beam

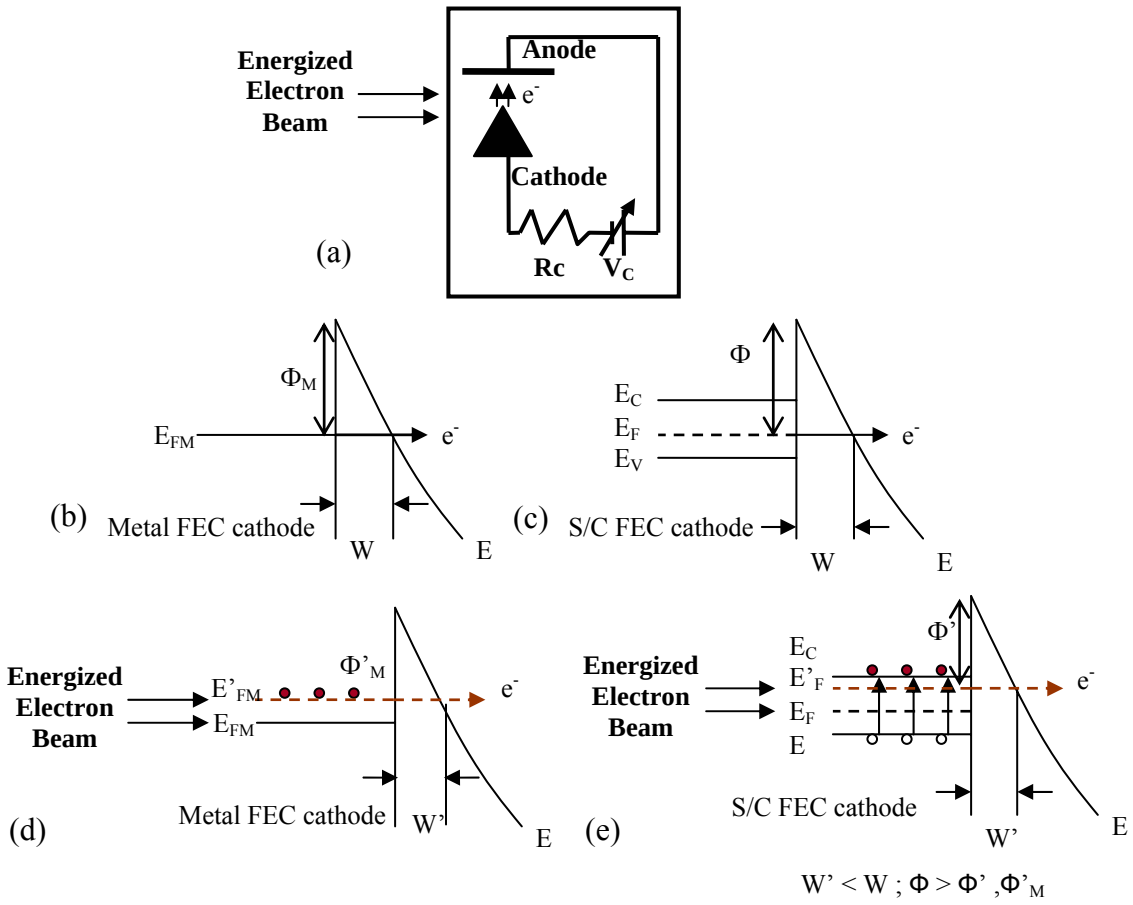

Figure 3.2: (a) Field emission cell with $V_c > V_{turn\text{-}on}$ under energized electron beam. Energy band diagram of (b) metal and (c) semiconductor FEC cathode without energized electron beam; Energy band diagram of (d) metal and (e) semiconductor FEC cathode bombarded by external e-beam

Device Fabrication

The CNT emitters were synthesized on polished aluminum nitride (AlN) as the base substrate. The fabrication process began with a coating of 1 μm thick polysilicon layer on AlN using low-pressure CVD followed by a 50 nm thick chromium (Cr) deposition using DC magnetron sputtering under a vacuum of ~$5x10^{-5}$ Torr, as shown in

Figure 3.2. Conventional photolithography was first performed to pattern the anode of the field emission cell and the external cathode. Next, wet Cr etching followed by polysilicon removal from the exposed area were performed using fluorine based reactive ion-etching (RIE) to get the device structure. After that, a second lithography was performed to pattern 100 μm thick lines for FEC and external e-beam CNT cathodes. Electron beam lithography (EBL) technique was used for higher precision, details of which can be found in appendix C. Later, 50 μm of titanium (Ti) as metal line, followed by 12 μm of cobalt (Co) was deposited as CNT growth catalyst. After resist removal in acetone, CNTs were synthesized using standard MPCVD process detailed elsewhere [34]. Figure 3.3 and 3.4 shows the 3-dimentional and cross sectional view of the device structure respectively.

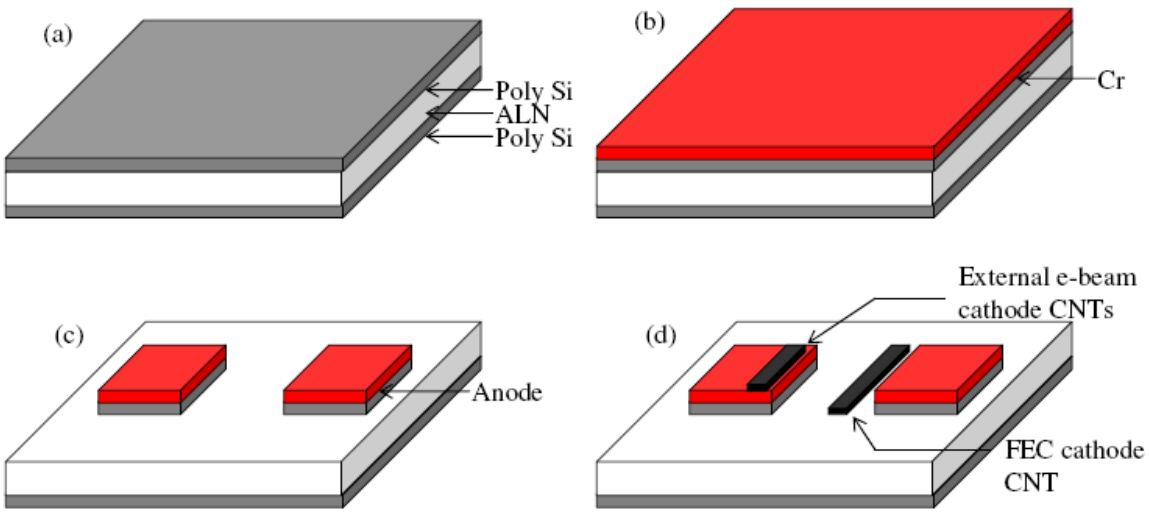

Figure 3.3: 3-D view of the device fabrication. (a) After polysilicon deposition on ALN, (b) after Cr deposition, (c) after Cr and polysilicon etching, (d) after e-beam patterning, catalyst deposition and CNT synthesis.

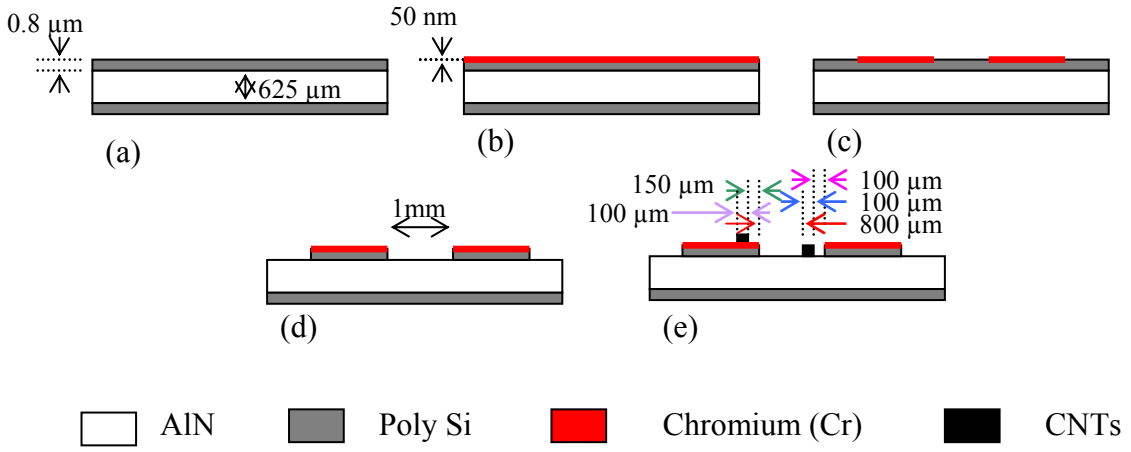

Figure 3.4: Cross sectional view of the device fabrication. (a) After polysilicon deposition on ALN, (b) after Cr deposition, (c) after Cr wet etching, (d) polysilicon etching and (e) after e-beam patterning, catalyst deposition and CNT synthesis.

Experiment

A schematic diagram of the complete test circuit is shown in Figure 3.5. A computerized data acquisition system equipped with labview program (National Instruments) was used to measure emission current (I) across R_a and R_c as a function of the applied potential (V). I-V characteristics were determined according to the Fowler-Nordheim field emission theory [43]. Generally the F-N equation closely approximates current-voltage behavior of relatively highly doped semiconductors and is frequently used to calculate field enhancement factor, material work function, etc. Here an approximation by Spindt et al. [44, 45] was used for the current I in terms of the operating voltage V, local field conversion factor β (m^{-1}) and work function Φ (eV), which is given by [45]:

$$I = aV^2 \exp(-b/V) \quad \text{……..……..(1)}$$

Where,

$$a = \frac{\alpha A \beta^2}{1.1\phi} \exp\left(\frac{1.44 \times 10^{-7} B}{\phi^{1/2}}\right) \quad \text{.......................... (2)}$$

$$b = \left(\frac{0.95 B \phi^{3/2}}{\beta}\right) \quad \text{.. (3)}$$

and A and B are dimensionless constants, A = 1.54 x 10^{-6} and B = 6.87 x 10^{7}. Whereas β is expressed as the ratio of field enhancement to the anode-cathode distance,

$$\beta = \frac{K_{tip}}{d_{cathode-anode}} \quad \text{... (4)}$$

Where, K_{tip} = E/ (V/d), represents the geometrical enhancement of electric field E (V/m) at the emitter tip. In the higher voltage regime, current is simply proportional to the square of the applied voltage [45] ($I=aV^2$).

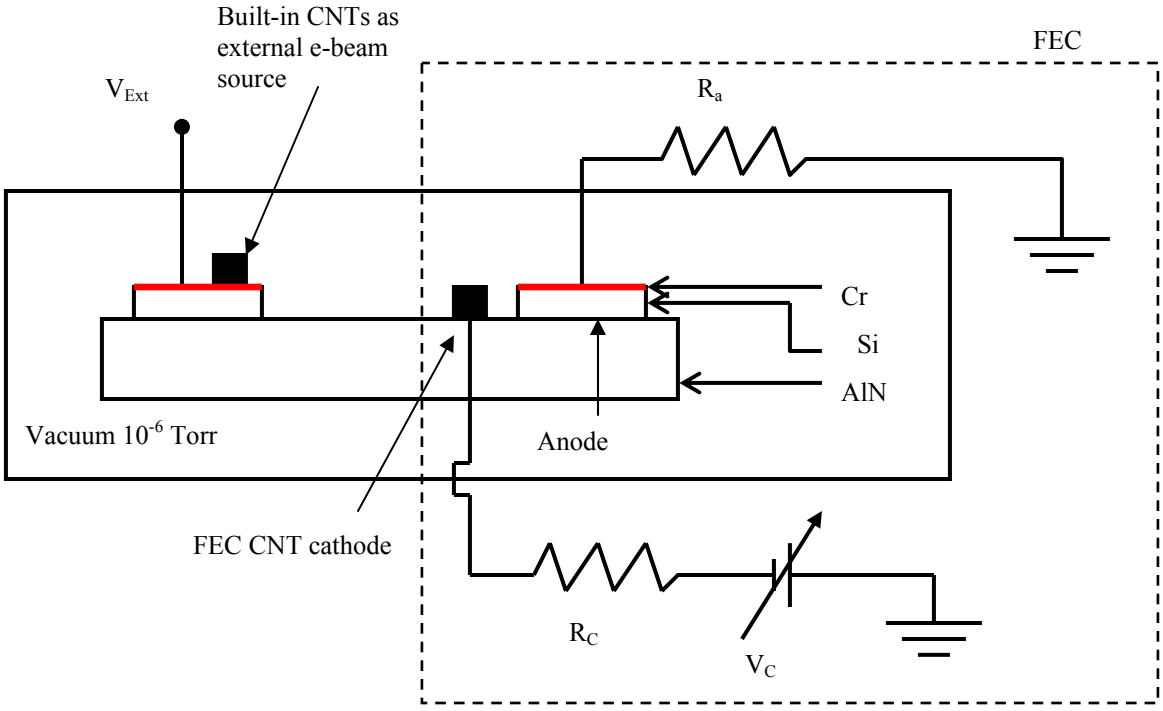

Figure 3.5: Schematic diagram of the complete electrical test circuit of the AFE device.

The fabricated single chip CNT amplified field emission (AFE) device was examined under Hitachi 4200 field emission scanning electron microscope (SEM), Figure 3.6. The CNTs were found to have an average diameter of ~20 nm and they are spaghetti-like. Field emission tests were performed at room temperature in a vacuum chamber evacuated to a base pressure of ~10^{-6} Torr. Three different test configurations were performed to characterize and electron emission from the FEC and external e-beam CNT cathodes.

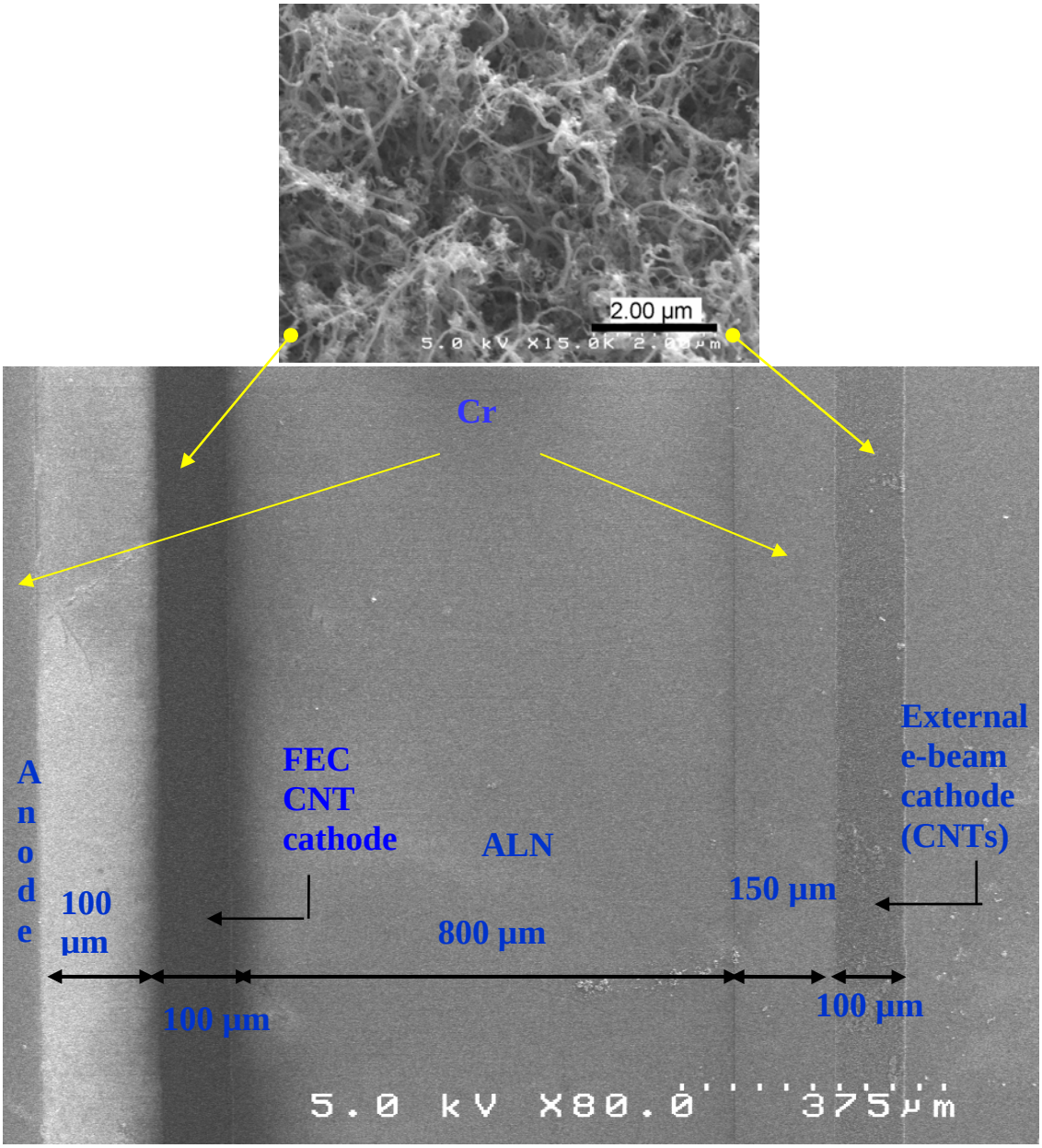

Figure 3.6: SEM micrograph of the AFE device structure. Top image shows high magnification inclined view of the CNTs.

Results and Discussions

Before imposing the external e-beam source on the FEC CNT cathode, I-V characteristics of the external source was determined with zero bias ($V_c = 0$)at the FEC cathode, Figure 3.7. In this circuit configuration, two different current components across R_c (I_{ExtC}) and R_a (I_{ExtA}) were measured as a function of the applied voltage. Field emission behavior is also confirmed by the corresponding F-N plots. Since the FEC cathode is closer to the external e-beam source than the FEC anode, most of the emitting electrons were captured by the FEC cathode. Due to this interference to the anode current, a change in the slopes of F-N plots is observed. Overall, the external e-beam delivered a total current ($I_{Ext}=I_{ExtC} + I_{ExtA}$) of ~12.5 nA to the FEC at 1.8 kV. Next, characterization of the FEC without external e-beam stimulator was performed, Figure 3.8. The FEC showed a turn-on field of ~2.7 V/μm for 1 nA of emission current (I_{FEC}) and increased exponentially to 4.5 nA at ~3.0 V/μm. I-V curve is plotted and the linearity of the corresponding F-N plot suggests field emission behavior is observed. Then, external e-beam source was imposed on the FEC CNT cathode and its potential was slowly varied from zero to 300 V while the external e-beam source was constantly operating at negative 1.8 kV, Figure 3.9 and 3.10. It can be noticed that, due to constant impact ionization the turn-on field of the FEC CNT cathode has reduced to 2.1 V/μm, Figure 3.11. Before the FEC cathode turns on, the current through R_c (I_{ExtC}) is due to the electrons collected by that cathode. I_{ExtC} slowly reduces with increasing FEC cathode bias, Figure 3.9 and 3.11. The reason being the net potential between external e-beam cathode and the FEC cathode decreases with increasing V_c, resulting in lesser current in

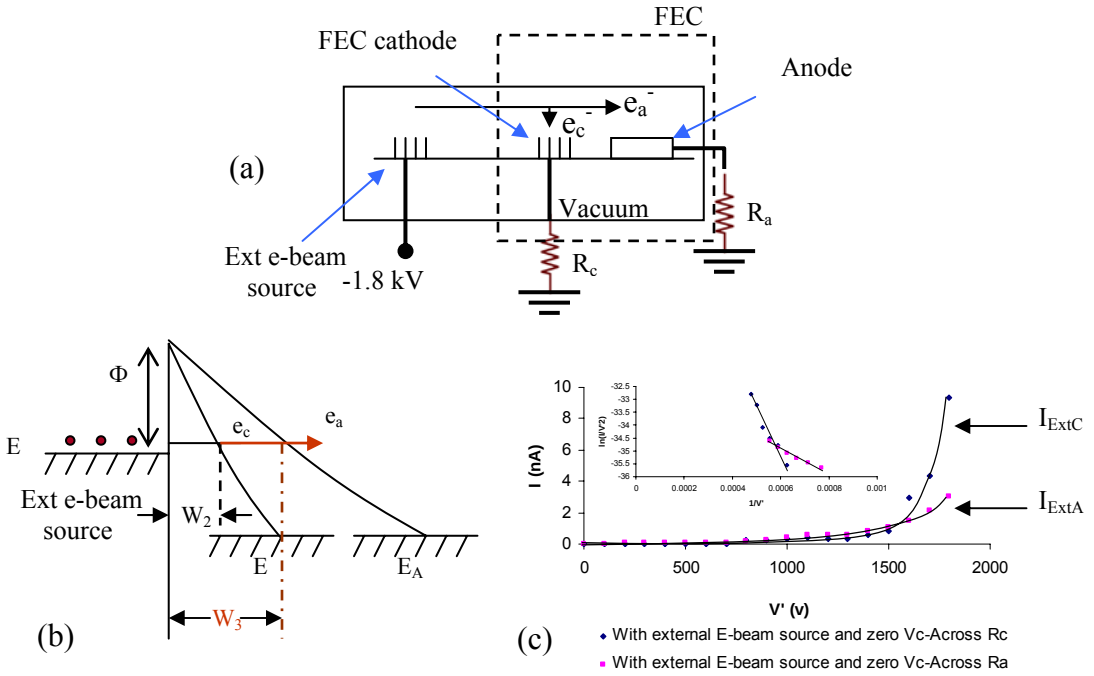

Figure 3.7: (a) Characterization of external e-beam source with FEC off. (b) Corresponding energy band diagram. (c) Corresponding I-V characteristics, inset shows the F-N plots.

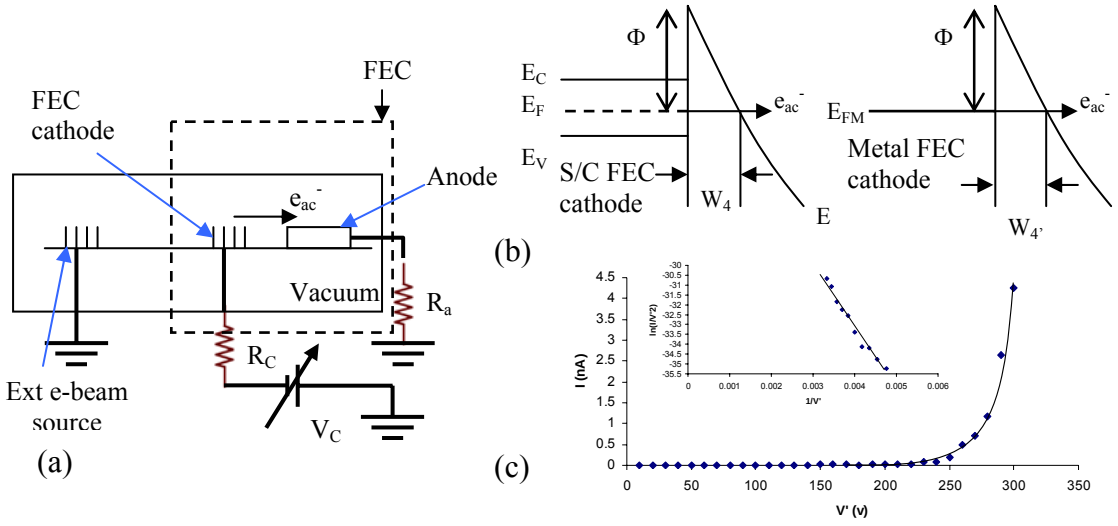

Figure 3.8: (a) Characterization of FEC w/o external e-beam bombardment. (b) Corresponding energy band diagram. (c) Corresponding I-V characteristics, inset shows the F-N plot.

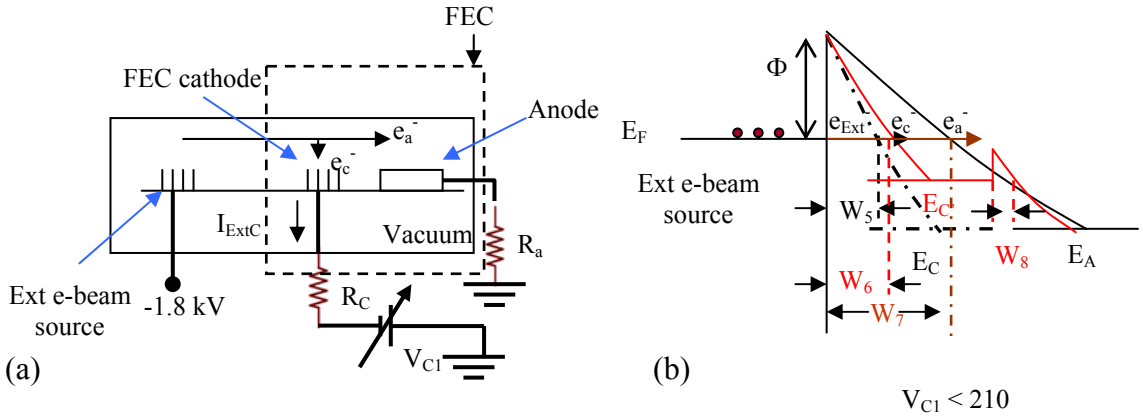

Figure 3.9: (a) Characterization of FEC: External e-beam ”on” and FEC biased but before turn-on, (b) Corresponding energy band diagram.

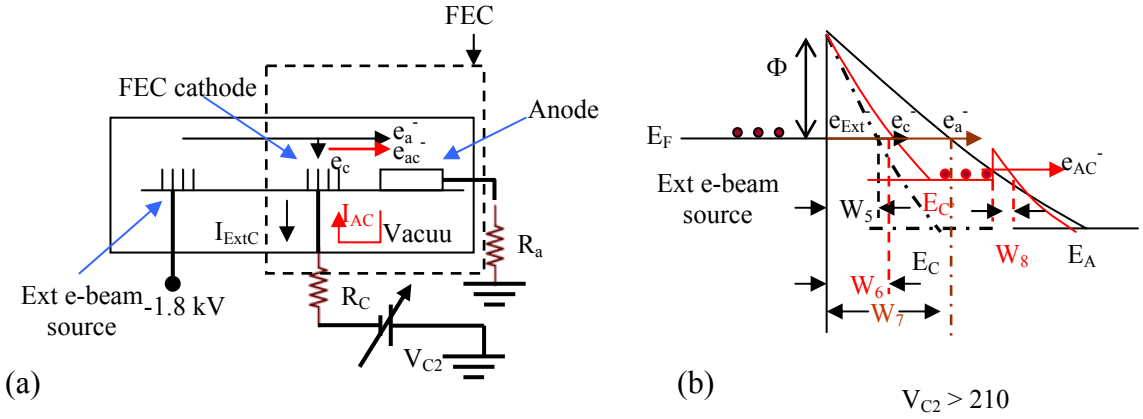

Figure 3.10: (a) Characterization of FEC: External e-beam ”on” and FEC turned-on, (b) Corresponding energy band diagram.

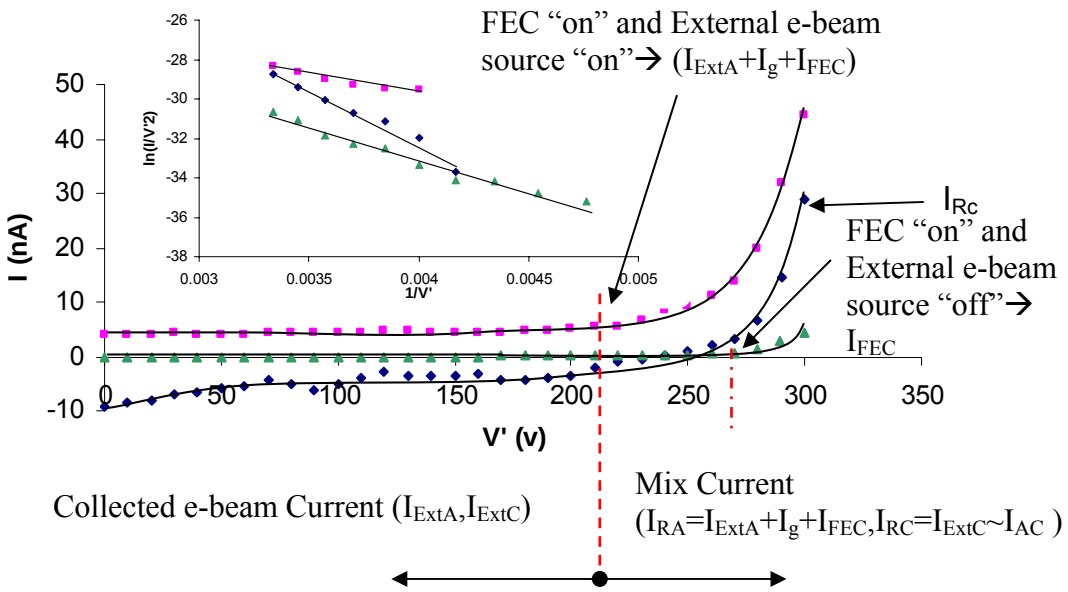

Figure 3.11: Comparison of Emission Currents; Current vs. Voltage (*I-V*) characteristics with different testing conditions. Inset shows the F-N plot of the corresponding emission data.

the circuit or in other words, with the increase in V_c, the tunneling barrier width also increases ($W_6 > W_5$) causing less electron tunneling through the potential barrier. Figure 3.9 (b) clearly explains this phenomenon, where E_c' is the field with increasing V_c. But when the FEC turns on, another current component starts flowing within the FEC (I_{AC}). So now, the current through the R_c is the resultant of these two current components ($I_{ExtC}\sim I_{AC}$). For simplicity it is assumed that current direction is same as that of electron flow. After the turn-on of the FEC, I_{AC} increased rapidly in an exponential manner with increasing FEC cathode bias and the resultant current changed its direction, Figure 3.11. This results in an exponential increase in anode current. Figure 3.10 (b) shows the tunneling of electrons across FEC potential barrier.

When operated in the AFE configuration with the external e-beam source biased at 1.8 kV, a total current (I_a) of 48 nA was delivered to the circuit at 300 V FEC cathode bias. I_a can be expressed as the sum of three different current components, i.e. $I_a = I_{extA} + I_g + I_{FEC}$, where I_g is the current due to the excess electron-hole pair generated by energized electron beam and it is assumed that I_{ExtC} is negligible small at maximum FEC cathode bias. Further, current gain is given by the ratio of amplified FEC current after turn-on ($I_g + I_{FEC}$) to the basic FEC current without external electron (I_{FEC}). Amplified FEC current is calculated by subtracting I_{extA} from the total current (I_a). Amplified FEC current ($I_g + I_{FEC}$) at 300 V is computed to be 45 nA which gives a current gain of 10. This gain clearly indicates that the amplified field emission behavior has been achieved successfully. In all the cases the emission behaviors are verified by corresponding F-N plots.

In AFE configuration, due to excess electron-hole pair generation by the energized electron beam source, the Fermi level moves closer to the conduction. As a result the work function of FEC CNT cathode has reduced. The new work function or sometimes called effective work function can be calculated as follow:

To start with let us consider the F-N equation [45]:

$$J = \frac{I}{A} = \mathrm{K}_1 \frac{F^2}{\phi} \exp\left[-\mathrm{K}_2 \frac{\phi^{\frac{3}{2}}}{F} \right] \quad \ldots\ldots\ldots\ldots\ldots\ldots\ldots\ldots\ldots\ldots (5)$$

where,

J (A/cm^2): Current density,

Φ (eV): Work function,

I (A): Emission current,

A (cm^2): Emission area,

$K_1 = e^3 / 8\pi h = 1.54 \times 10^{-6}$ $AeVV^{-2}$,

$K_2 = 4(2m_e)^{1/2} / 3e\hbar = 6.83 \times 10^7$ $eV^{-3/2}Vcm^{-1}$,

and F is the local electric field which is given by,

$$F = \beta E \quad \text{……..……(6)}$$

where $E = V/d$ (V/cm) is the macroscopic field, V (V) is the applied voltage between two planar parallel electrodes separated by a distance d (cm), and β is the field enhancement or amplification factor. β is determined by the geometrical shape and the surroundings of the emitter, such as surface contaminants and defects [16].

Taking natural logarithm on both sides of Eq. 4 and substituting F, we have:

$$\ln\left\{\frac{I}{E^2}\right\} = \ln\left\{\frac{K_1 A\beta^2}{\phi}\right\} - \frac{K_2\phi^{3/2}}{\beta E} \quad \text{..……..(7)}$$

By comparing Eq. 6 with an equation of a straight line (y = mx + c), we have:

$$\text{Slope of the F-N plot (m)} = -\frac{K_2\phi^{\frac{3}{2}}}{\beta} \quad \text{…….……..(8)}$$

Now if, $m_{FE(w)}$ and $m_{FE(w/o)}$ be the slopes of F-N plots, Figure 3.12 (b), for with and without external stimulator then their ratio is given by (assuming β doesn't change),

$$\frac{m_{FE(w/o)}}{m_{FE(w)}} = \left(\frac{\phi_{FE(w/o)}}{\phi_{FE(w)}} \right)^{\frac{3}{2}} \quad \text{.....(9)}$$

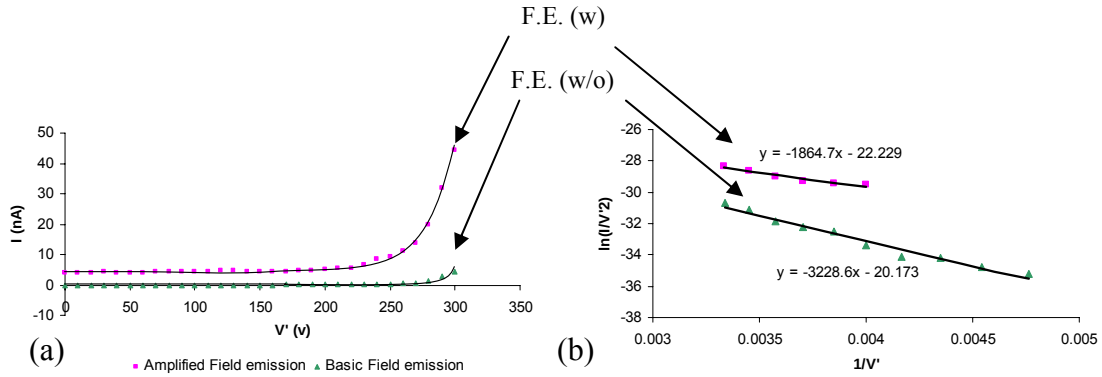

Figure 3.12: (a) Current vs. Voltage characteristics of with and without external stimulator. (b) F-N plots of the corresponding emission data.

Usually the surface potential barrier or work function (Φ) of multiwalled CNT is ~5 eV [35]. So, Eq. 9 gives, $\Phi_{FE(w)} = 3.46$ eV.

Consequently it is concluded that the proposed amplified field emission behavior has been achieved.

CHAPTER IV

SUMMARY AND CONCLUSIONS

In the first part of the research, multiwalled vertically aligned CNTs have been successfully synthesized by using MPCVD method which has been regarded as one of the most promising candidates for the synthesis of CNTs. It is observed that many physical parameters such as different gas combinations and flow rates, buffer layer thickness, order of pretreatment, variations in growth temperature, microwave power and growth time can influence the CNT growth. There exists a particular ratio of hydrocarbon to hydrogen which highly affects the alignment and quality of CNTs. With the hydrocarbon fraction ranges from 8-13 %, the length of the CNTs ranges from 10-50 μm while the diameters are ~ 40 nm. The applied microwave power, thickness of the buffer layer and the catalyst film also play an important role. Proper pretreatment order, time and temperature reduce the amount of nano-carbon particles deposition, and keep the catalytic particles active during the growth period. A negative bias was also applied successfully to grow more aligned CNTs. Turning off the carbon containing gas few seconds before turning off the plasma helps to get cleaner CNTs. Overall, the encouraging results demonstrated thus far in this discussion show that aligned CNTs can be grown under different conditions by MPCVD method. The findings from the set of experiments can be extremely helpful to implement CNTs successfully in practical applications such as vacuum microelectronics devices and sensors. These important findings are implemented in developing CNT field emission cell with built-in electron beam source.

.In this part, a single chip CNT field emitter with integrated metallic anode was fabricated and their field emission property was first tested without any external stimulator. Later it was investigated that how the electron emission process can be stimulated using another electron beam that hits the emitting CNTs. Higher electric field was used to generate the bombarding electron beam source. The emission current of the FEC increases markedly with the external e-beam stimulator due to the impact ionization of the external e-beam with the FEC CNT cathode. I-V curves were plotted and the emission behaviors were confirmed by the corresponding F-N plots. It was found that almost 10 times higher current was achieved energized electron beam source. Overall, these results demonstrate the feasibility of a novel means of power generation using electron stimulated impact ionization field emission.

CHAPTER V

RECOMMENDATIONS

Preliminary results of CNT synthesis by microwave plasma-enhanced CVD (MPCVD) and CNT field emission cell with built-in electron beam source have shown good field emission behavior and current amplification. However there is a tremendous scope of improvement in the performance of the electrodes. The present studies can be further extended to include the following:

- Transmission electron microscopy (TEM) analysis of the CNTs – to analyze the actual tube diameter, number of shell/ walls, defects and amorphous carbon incorporation.
- Raman spectra of the synthesized CNTs.
- The effect of different catalyst such as Ni, Fe and Pd on the morphology, Raman spectra and field emission characteristics.
- Study the catalyst after pretreatment to obtain well aligned CNTs.
- Applying higher DC bias by the modification of the PECVD system to help taller and more vertically aligned CNTs.
- Optimization of the gaps between the electrodes to achieve higher current amplification.
- Synthesize more vertically aligned CNTs to get more stable emission current.
- Enhancement of the quantum efficiency of the AFE cell.

- Cleaning treatment on CNTs – to reduce amorphous carbon contaminations which help to get better emission.
- Determine the quantum efficiency of the FEC.
- Investigate the potential use of the electron beam stimulated amplified field emission for energy conversion application.

APPENDIX A

Structure and Properties of Carbon Nanotubes

CNTs are carbon nanostructured materials, which have been widely regarded as an emerging material for nanoscale science and engineering research. The advantages of using CNTs as emitter can be understood by their structure and properties [1, 15, and 28], as listed below:

A. Structures

- Bonding: sp^2 hybrid orbital allows carbon atoms to form hexagon and sometimes pentagon or heptagon units by in plan σ bonding and out-of-plane π bonding.
- Defect-free nanotubes: Tabular structure of carbon atoms of hexagonal network. Tube curvature results in σ-π rehybridization or mixing.
- Defective nanotubes: Occasionally pentagons and heptagons are incorporated into a hexagonal network of carbon atoms to form bent, branched, coroidal, and helical or capped nanotubes. The mechanical and electrical properties of CNTs are highly depending on their diameter and structural defects.

B. Properties:

- Electrical: Defect-free nanotubes behave like either semiconductor or metallic with quantized conductance due to electron confinement along the tube circumference, whereas pentagon or heptagons will generate localized states.

- Optical and optoelectronic: One-dimensional band structure and direct band gap make nanotubes ideal for optical applications with wave length ranging between 300 to 3000 nm.
- Mechanical and electromechanical: σ-π rehybridization gives nanotubes the maximum Young's modulus of over 1 TPa and tensile strength of over 100 GPa. It gives extremely good responses to strain and metal-insulator transition.
- Magnetic and electromagnetic: Electron orbits circulating around nanotubes give rise to many interesting phenomenon such as metal-insulator transition and quantum oscillation.
- Chemical and electrochemical: High specific surface facilitate molecular absorption, doping and charge transfer on nanotubes, which indirectly enhance electronic properties.
- Thermal and thermoelectric: Nanotubes display highest thermal conductivity (inherited from graphite) whiles the quantum effects are observed at low temperature.

Table A.1 provides some of the important properties of CNTs and compares them with that of undoped diamond and silicon.

Table A.1: Important properties of CNTs

Physical Properties	**CNTs [47]**	**Diamond [48,49]**	**Si [48,49]**
Young's Modulus (TPa)	~1	~1.22	0.15
Tensile Strength (GPa)	~200	> 1.2	3.7
Thermal Conductivity (W/cmK)	~20	~20	~1.5
Density (g/cm3)	~1.4	3.52	2.32
Resistivity (Ω-cm)	~10-4	10^{12}-10^{16} (undoped)	2.3 x 10^{5} (undoped)
Electron Affinity (eV)	~4.8	NEA / Small	4.05
Energy Band Gap (eV)	~0.7-0.9	~5.45	1.12

APPENDIX B

Growth Mechanism of Carbon Nanotubes

The way in which nanotubes are formed is not exactly known. The growth mechanism is still a subject of controversy, and more than one mechanism might be operative during the formation of CNTs. There are several theories on the exact growth mechanism for nanotubes. One theory [50] postulates that metal catalyst particles are floating or are supported on graphite or another substrate. It presumes that the catalyst particles are spherical or pear-shaped, in which case the deposition will take place on only one half of the surface (this is the lower curvature side for the pear shaped particles), as shown in Figure B.1. The carbon diffuses along the concentration gradient and precipitates on the opposite half, around and below the bisecting diameter. However, it does not precipitate from the apex of the hemisphere, which accounts for the hollow core that is characteristic of these filaments. For supported metals, filaments can form either by "extrusion (also known as base growth)" in which the nanotube grows upwards from the metal particles that remain attached to the substrate, or the particles detach and move at the head of the growing nanotube, labeled "tip-growth". Depending on the size of the catalyst particles, SWNT or MWNT are grown. This mechanism is based on in-situ TEM observations [51].

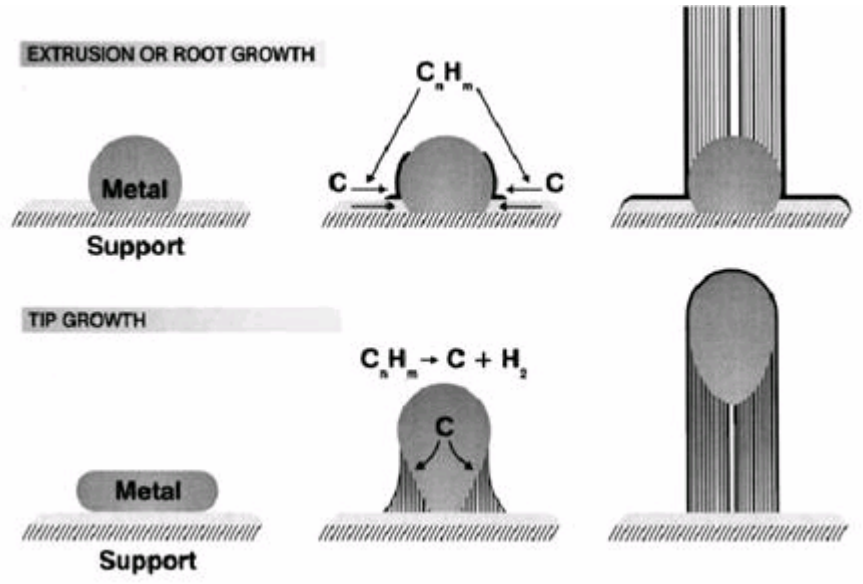

Figure B.1: Visualization of a possible carbon nanotube growth mechanism.

Synthesis of Carbon Nanotubes

In this section, different techniques for nanotube synthesis are briefly explained. They are generally produced by three main techniques, arc discharge, laser ablation and chemical vapor deposition. Though, scientists are researching to find more economic ways to produce these structures.

Arc Discharge:

This method creates nanotubes through arc-vaporization of two carbon rods placed end to end, separated by approximately 1mm, in an enclosure that is usually filled with inert gas (helium, argon) at low pressure (between 50 and 700 mbar) [52]. A basic schematic of a typical arc-discharge system is shown in Figure B.2. Recent investigations have shown that it is also possible to create nanotubes with the arc method in liquid nitrogen [53] and in a magnetic field [54]. A direct current of 50 to 100 A driven by

approximately 20 V creates a high temperature discharge between the two electrodes. The discharge vaporizes one of the carbon rods and forms a small rod shaped deposit on the other rod. Producing nanotubes in high yield depends on the uniformity of the plasma arc and the temperature of the deposit form on the carbon electrode [52].

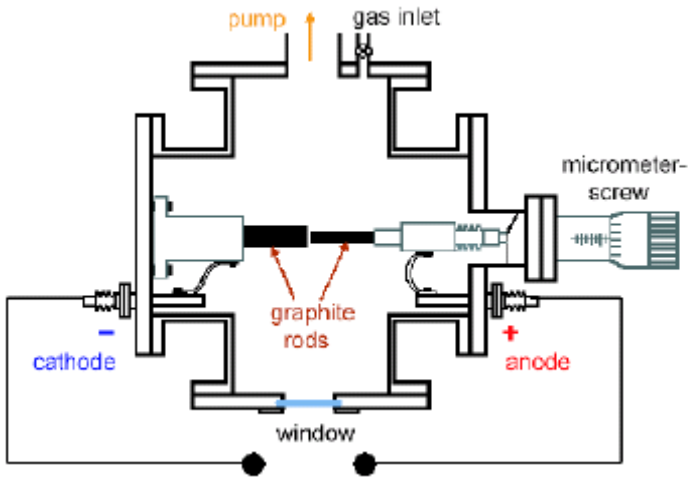

Figure B.2: Schematic of a typical arc-discharge system

Laser Ablation:

In 1995, Smalley's group [55] at Rice University reported the synthesis of carbon nanotubes by laser vaporization. The laser vaporization apparatus used by Smalley's group is shown in Figure B.3. A pulsed [56, 57], or continuous [58, 59] laser is used to vaporize a graphite target in an oven at 1200 °C. The main difference between continuous and pulsed laser, is that the pulsed laser demands a much higher light intensity (100 kW/cm^2 compared with 12 kW/cm^2). The oven is filled with helium or argon gas in order to keep the pressure at 500 Torr. A very hot vapor plume forms, then expands and cools

rapidly. As the vaporized species cool, small carbon molecules and atoms quickly condense to form larger clusters, possibly including fullerenes. The catalysts also begin to condense, but more slowly at first, and attach to carbon clusters and prevent their closing into cage structures [60]. Catalysts may even open cage structures when they attach to them. From these initial clusters, tubular molecules grow into single-wall carbon nanotubes until the catalyst particles become too large, or until conditions have cooled sufficiently that carbon no longer can diffuse through or over the surface of the catalyst particles. It is also possible that the particles become that much coated with a carbon layer that they cannot absorb more and the nanotube stops growing. The SWNTs formed in this case are bundled together by van der Waals forces [60]

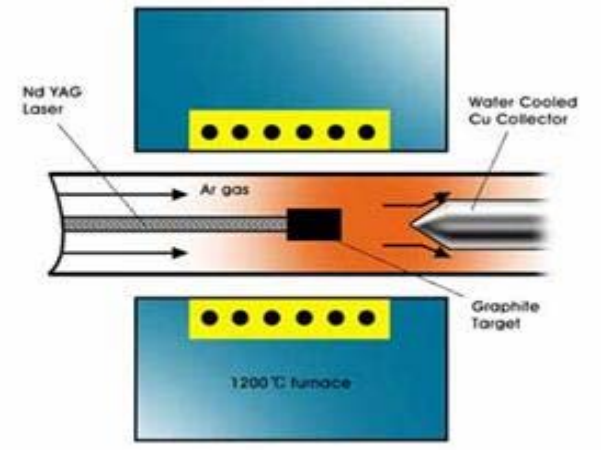

Figure B.3: The laser vaporization apparatus used by Smalley's group.

Chemical Vapor Deposition:

CVD carbon nanotube synthesis is essentially a two-step process consisting of a catalyst preparation step followed by the actual synthesis of the nanotube. It is achieved by putting a carbon source in the gas phase and using an energy source, such as plasma or a resistively heated coil, to transfer energy to a gaseous carbon molecule. Commonly used gaseous carbon sources include methane, carbon monoxide and acetylene. The energy source is used to "crack" the molecule into reactive atomic carbon [1, 61]. Then, the carbon diffuses towards the substrate, which is heated and coated with a catalyst (usually a first row transition metal such as Ni, Fe or Co) where it will bind. Carbon nanotubes will be formed if the proper parameters are maintained. Excellent alignment [61], as well as positional control on nanometre scale [62], can be achieved by using CVD. Control over the diameter, as well as the growth rate of the nanotubes can also be maintained. A schematic of plasma enhanced CVD (PECVD) system, owned by Vanderbilt University to grow CNTs is shown in Figure B.4.

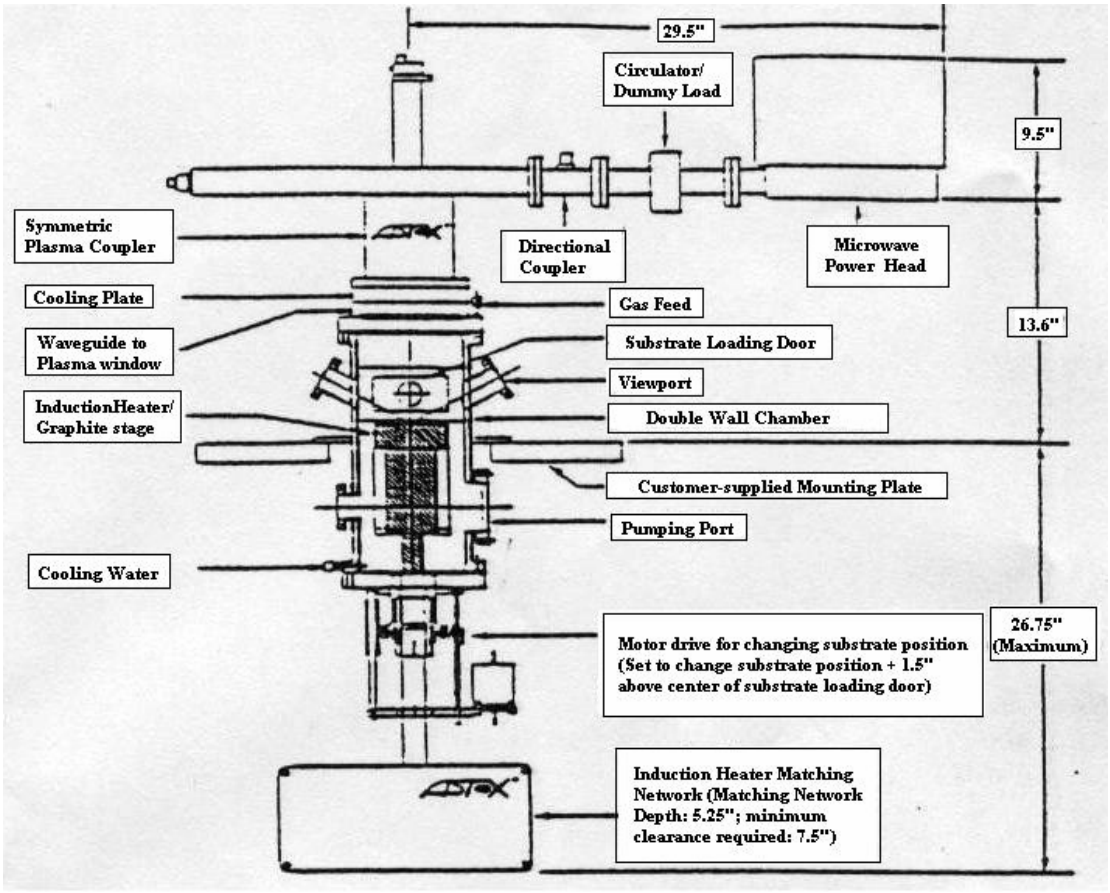

Figure B.4: Schematic of plasma enhanced CVD (PECVD) system.

APPENDIX C

Electron Beam Lithography

Electron beam lithography (often abbreviated as e-beam lithography) is the practice of a lithography process by scanning a beam of electrons in a patterned fashion across a surface covered with a film, called the resist ("exposing" the resist) and of selectively removing either exposed or non-exposed regions of the resist ("developing"). Just like optical lithography, electron lithography also uses positive and negative resists, which in this case are referred to as electron beam resists (or e-beam resists). E-beam resists are e-beam-sensitive materials that are used to cover the wafer according to the defined pattern.

A typical EBL system consists of the following parts [63, 64]: 1) an electron gun or electron source that supplies the electrons; 2) an electron column that 'shapes' and focuses the electron beam; 3) a mechanical stage that positions the wafer under the electron beam; 4) a wafer handling system that automatically feeds wafers to the system and unloads them after processing; and 5) a computer system that controls the equipment. A picture of a EBL system is shown in Figure C.1.

The primary advantage of electron beam lithography is that it is one of the ways to beat the diffraction limit of light and make features in the nanometer regime. This form of maskless lithography has found wide usage in mask-making used in photolithography, low-volume production of semiconductor components, and research & development. On the other hand, the key limitation of electron beam lithography is throughput, i.e., the very long time it takes to expose an entire silicon wafer or glass substrate. A long

exposure time leaves the user vulnerable to beam drift or instability which may occur during the exposure. Also, the turn-around time for reworking or re-design is lengthened unnecessarily if the pattern is not being changed the second time.

Figure C.1: A typical Electron Beam Lithography system.

REFERENCES

[1] M. Meyyappan, Carbon Nanotubes Science And Applications, CRC Press, 2-21

[2] Oberlin, A.; M. Endo, and T. Koyama, J. Cryst. Growth (March 1976). "Filamentous growth of carbon through benzene decomposition" 32: 335–349. doi:10.1016/0022-0248(76)90115-9. Retrieved on 2007-07-28

[3] Endo, Morinobu & Dresselhaus, M. S. (October 26, 2002), Carbon Fibers and Carbon Nanotubes (Interview, Nagano, Japan), Retrieved on 26 July 2007

[4] W.B. Choi, D.S. Chung, J.H. Kang, H.Y. Kim, Y.W. Jin, I.T. Han, Y.H. Lee, J.E. Jung, N.S. Lee, G.S. Park, J.M. Kim, Appl. Phys. Lett. 75 (1999) 3129

[5] J. Robertson, W.I. Milne, K.B.K. Teo, M. Chhowalla, "Fielld emission application of carbon nanotubes", XVI International Winterschool on Electronic Properties of Novel Materials, Kirchberg, Austria, 2002 (2–9 March), pp. 537–542

[6] Y.M. Wong, W.P. Kang, J.L. Davidson, A. Wisitsora-at, K.L. Soh, Sens. Actuators, B 93 (2003) 326–331

[7] J. Hafner, C. Cheung, C. Lieber, Nature 398 (1999) 761

[8] S.J. Tans, M.H. Devoret, H. Dai, A. Thess, R.E. Smalley, L.J. Geerlings, C. Dekker, Nature 386 (1997) 474

[9] C. Lui, Y.Y. Fan, M. Lui, H.T. Cong, M.S. Dresselhaus, "Hydrogen storage in single-walled carbon nanotubes at room temperature", Science 286 (1127) (1999)

[10] R. Rosen, W. Simendinger, C. Debbault, H. Shimoda, L. Fleming, B. Stoner, and O. Zhuo, Appl. Phys. Lett. 76 (2000) 1668-1670

[11] C. Nui, E. K. Sichel, R. Hoch, D. Moy, and H Tennent, Appl. Phys. Lett. 70 (1997) 1480

[12] T. Rueckes, K. Kim, E. joselevich, G. Y. Tseng, C. L. Cheung, and C. M. Lieber, Science 289 (2000) 94-97

[13] P. Kim and C. M. Lieber, Science 286 (1999) 2148-2150

[14] S.J. Wind, J. Appenzeller, R. Martel, and P. Avouris, "Vertical scaling of carbon nanotube field-effect transistors using top gate electrodes", Appl. Phys. Lett. 80 (2002) 3817

[15] M. Daenen, R. D. de Foue, B. Hamers, P. G. A. Janssen, K. Schouteden, and M. A. J. Veld, “The wonders world of carbon nanotubes”, 27 February 2003

[16] Y. M. Wong, Master’s Thesis, “Fabrication and characterization of carbon nanotubes field emission cathodes grown by CVD with palladium as catalyst”, Vanderbilt University

[17] M. Meyyappam, Carbon Nanotubes Science And Applications, CRC Press, 99-112, 117-134, 163-187, 195-211

[18] W. Zhu, “Vacuum Microelectronics”, John Wiley & Sons, 2001

[19] W. Zhu, C. Bower, G. P. Kochanski, and S. Jin, “Field emission properties of diamond and carbon nanotubes”, Diamond and related Materials 10 (2001) 1709-1713

[20] M.J. Yacaman, M.M. Yoshida, L. Rendon, J.G. Santiesteban, Appl. Phys. Lett. 62 (1993) 657

[21] Y.M. Wong, S. Wei, W.P. Kang, J.L. Davidson, W. Hofmeister, J.H. Huang, Y. Cui, Diamond & Related Materials 13 (2004) 2105-2112

[22] S. Wei, W.P. Kang, J.L. Davidson, J.H. Huang, Diamond & Related Materials 15 (2006) 1828-1833

[23] Mi Chen, Chieng-Ming chen, Horong-Show koo, Chia-Foo Chen, Diamond & Related Materials 12 (2003) 1829-1835

[24] E.F. Kukovitsky, S.G. L’vov, N.A. Sainov, V.A. Shustov, L.A. Chernozatonskii, Chem. Phys. Lett. 355 (2002) 497

[25] H.J. Dai, A.G. Rinzler, P. Nikolaev, A. Thess, D.T. Colbert, R.E. Smalley, Chem. Phys. Lett. 260 (1996) 471

[26] A. Fonseca, K. Hernadi, P. Piedigrosso, et al., Electrochem. Soc. 97 (1997) 884

[27] Y.M. Wong, W.P. Kang, J.L. Davidson, B.K. Choi, W. Hofmeister, J.H. Huang, Diamond & Related Materials 14 (2005) 2069-2073

[28] A.V. Melechko, V.E. Merkulov, M.A. Guillorn, K.L. Klein, D.H. Lowndes, M.L. Simpson, Journal of Applied Physics 97, 041301, 2005

[29] Y. Hayashi, T. Tokunaga, S. Toh, W.-J. Moon, K. Kaneko, Diamond & Related Materials 14 (2005) 790– 793

[30] C.L. Tsai, C.F. Chen, Diamond and Related Materials 12 (2003) 1615–1620

[31] K. Bartsch, B. Arnold, R. Kaltofen, C. Taschner, J. Thomas, A. Leonhardt, Carbon 45 (2007) 543–552

[32] Siang-Piao Chai, Sharif Hussein Sharif Zein, Abdul Rahman Mohamed, Carbon 45 (2007) 1535–1541

[33] Chao Hsun Lin, Hui Lin Chang, Chih Ming Hsu, An Ya Lo, Cheng Tzu Kuo, Diamond & Related Materials 12 (2003) 1851-1857

[34] Y.M. Wong, W.P. Kang, J.L. Davidson and J.H. Huang, Diamond and Related Materials 15 (2006) 1859-1862

[35] K. Subramanian, Y.M. Wong, W.P. Kang, J.L. Davidson, B.K. Choi and M. Howell, Diamond and Related Materials 16 (2007) 1997-2002

[36] Kun Hou, Ronald A. Outlaw, Sigen Wang, Mingyao, Ronald A. Quinlan, Dennis M. Manos, Maetin E. Kordesch, Uwe Arp and Brian C. Holloway, Applied Physics Letter 92, 133112, 2008

[37] H.Y. Fan, Physical Review Vol. 68, Numbers 1 and 2

[38] A.A. Dadykin, A.G. Naumovets, Yu.N. Kozyrev,M.Yu. Rubezhanska, P.M. Lytvyn, Yu.M. Litvin, Progress in Surface Science 74 (2003) 305–318

[39] Alireza Nojeh, Wai-Kin Wong, Eric yieh, R. Fabian Pease, Hongiee Dai, J. Vac. Sci Technol. B, 22(6), Nov/Dec 2004

[40] Robert F. Pierret, Modular Series on Solid State Devices, Semiconductor Fundamentals (Vol. 1)

[41] R. Zimmermann, K. Karl, Phys. Stat. Sol. (b) 160, K109 (1990)

[42] http://en.wikipedia.org/wiki/Phonon

[43] R.H. Fowler and L.W. Nordheim, Proc. R. Soc. London, Ser. A 119, 173 (1928)

[44] C.A. Spindt, I. Brodie, L. Humphrey and E.R. Westerberg, J. Appl. Phy., Vol. 47, pp. 5284-5263

[45] Veljko Milanovic, IEEE, Transaction on Devices, Vol. 48, No. 1, January 2001

[46] Y.M. Wong, W.P. Kang, J.L. Davidson, B.K. Choi and J.H. Huang, J. Vac. Sci Technol. B, 25(2), Mar/Apr 2007

[47] http://www.pa.msu.edu/cmp/csc/ntproperties/ and Kazaoui et al., Appl. Phys. Lett. 78 (2001) 3433

[48] T. A. Railkar, W. P. Kang et al., Critical Reviews in Solid State and Materials Sciences 25 (2000) 163

[49] J.E. Field, "The Properties of Natural and Synthetic Diamond", Academic Press, London, 1992

[50] S. B. Sinnot et al., *Chem.Phys.Lett.* 315, 25-30 (1999)

[51] Yasuda, Ayumu, Kawase, Noboru, and Mizutani, Wataru. "Carbon-Nanotube Formation Mechanism Based on in Situ TEM Observations." Journal of Physical Chemistry B 106(51), 13294-13298. 2002

[52] T. W. Ebbesen and P. M. Ajayan, Nature 358, 220-222 (1992)

[53] S. H. Jung et al., Applied Physics A-Materials Science & Processing 76, 285-286 (2003)

[54] Anazawa, Kazunori, Shimotani, Kei, Manabe, Chikara, Watanabe, Hiroyuki, and Shimizu, Masaaki. "High-purity carbon nanotubes synthesis method by an arc discharging in magnetic field." Applied Physics Letters 81(4), 739-741. 2002

[55] Guo, T., Nikolaev, P., Thess, A., Colbert, D. T., and Smalley, R. E. "Catalytic growth of single-walled nanotubes by laser vaporization." Chemical Physics Letters 243(1,2), 49-54. 1995

[56] Yudasaka, M., Yamada, R., Sensui, N., Wilkins, T., Ichihashi, T., and Iijima, S. "Mechanism of the Effect of NiCo, Ni and Co Catalysts on the Yield of Single-Wall Carbon Nanotubes Formed by Pulsed Nd:YAG Laser Ablation." Journal of Physical Chemistry B 103(30), 6224-6229. 1999

[57] Eklund, P. C., Pradhan, B. K., Kim, U. J., Xiong, Q., Fischer, J. E., Friedman, A. D., Holloway, B. C., Jordan, K., and Smith, M. W. "Large-Scale Production of Single-Walled Carbon Nanotubes Using Ultrafast Pulses from a Free Electron Laser." Nano Letters 2(6), 561-566. 2002

[58] Maser, W. K., Munoz, E., Benito, A. M., Martinez, M. T., de la Fuente, G. F., Maniette, Y., Anglaret, E., and Sauvajol, J. L. "Production of high-density single-walled nanotube material by a simple laser-ablation method." Chemical Physics Letters 292(4,5,6), 587-593. 1998

[59] Bolshakov, A. P., Uglov, S. A., Saveliev, A. V., Konov, V. I., Gorbunov, A. A., Pompe, W., and Graff, A. "A novel CW laser-powder method of carbon single-wall nanotubes production." Diamond and Related Materials 11(3-6), 927-930. 2002

[60] Scott, C. D., Arepalli, S., Nikolaev, P., and Smalley, R. E. “Growth mechanisms for single-wall carbon nanotubes in a laser-ablation process.” Applied Physics A: Materials Science & Processing 72(5), 573-580, 2001

[61] Ren, Z. F., Huang, Z. P., Xu, J. W., Wang, J. H., Bush, P., Siegel, M. P., and Provencio, P. N. “Synthesis of large arrays of well-aligned carbon nanotubes on glass.” Science (Washington, D.C.) 282(5391), 1105-1107, 1998

[62] Ren, Z. F., Huang, Z. P., Wang, D. Z., Wen, J. G., Xu, J. W., Wang, J. H., Calvet, L. E., Chen, J., Klemic, J. F., and Reed, M. A. “Growth of a single freestanding multi-wall carbon nanotube on each nano-nickel dot.” Applied Physics Letters 75(8), 1086-1088, 1999

[63] http://www.siliconfareast.com/lith_electron.htm

[64] http://en.wikipedia.org/wiki/Electron_beam_lithography